Towards battery separator films: Production of Solid-State PEI Nanofoams Using Supercritical CO_2

Brian Aher

A thesis

submitted in partial fulfillment of the

requirements for the degree of

Master of Science in Mechanical Engineering

University of Washington

2012

Committee:

Vipin Kumar

Junlan Wang

John Weller

Program Authorized to Offer Degree:

Mechanical Engineering

Table of Contents

List of Figures

List of Tables

Acknowledgements

The author wishes to acknowledge the significant contribution of Professor Vipin Kumar to the success of this research. His expertise, encouragement, and resources were instrumental in this pursuit. The author also owes a great debt of gratitude to the present and former members of the Microcellular Plastics Laboratory, especially Huimin Guo, for their friendship, selflessness, and inspiration. In addition, this thesis was made possible by the unflagging support of my family and loved ones.

Dedication

I dedicate this work to my brother.

Chapter 1 Introduction

1.1 Microcellular and Nanocellular Foams

Microcellular foams are thermoplastic foams with cells on the order of 10 μm in diameter. Typical microcellular foams have a cell density of 10^8 cells per cubic centimeter. The presence of these cells reduces the density of the foam by anywhere from 1-90%. Figure 1.1 shows a typical microcellular foam structure with closed cells. Microcellular foams typically have a cellular internal structure with a solid outer skin layer.

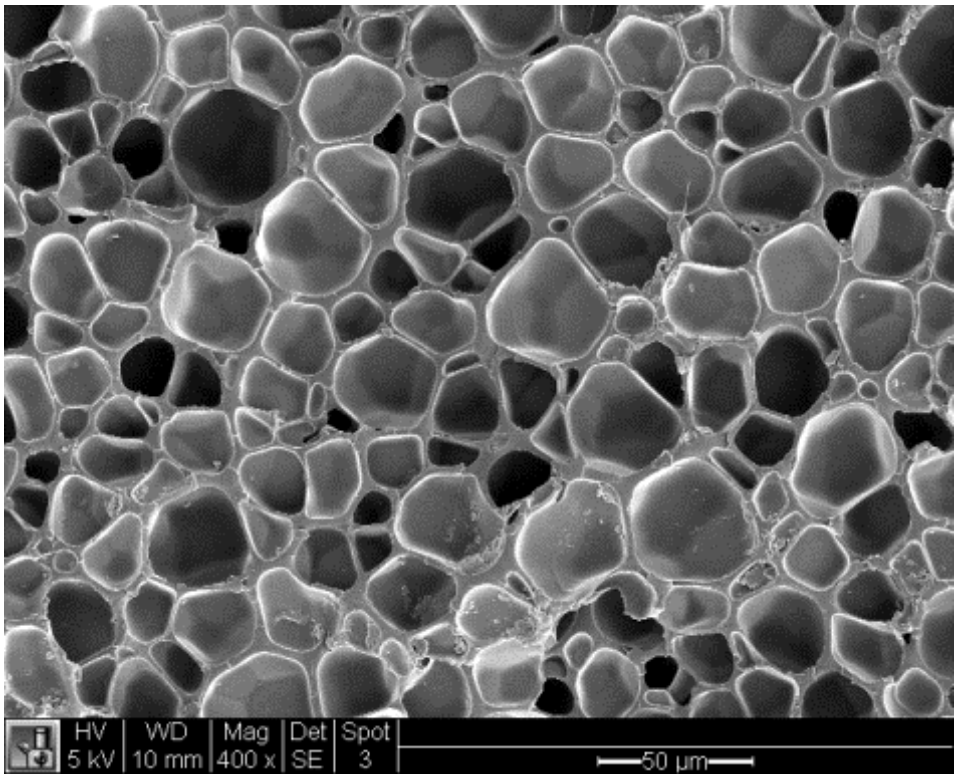

Figure 1.1: A scanning electron microscope image of a cross-section of microcellular foam with cell diameters on the order of 10 μm.

Microcellular foam was first created by Suh et al. at MIT in the early 1980's as a novel material for use in food packaging [1]. The motivation behind this invention was to reduce the material costs of food packaging parts without the significant sacrifice of strength found in

traditional foaming processes [2]. Conventional large cell foams, such as Styrofoam, have poor, unpredictable mechanical properties due to the large cell size relative to the part thickness. By contrast, microcellular foams of similar density reductions have cells that are orders of magnitude smaller than the part thickness, leading to better, more predictable mechanical properties.

Nanocellular foams are similar to microcellular foams, but have average cell diameters on the order of 10-100 nm and cell densities on the order of 10^{14}. Nanocellular foams were developed more recently as a refinement of the process for creating microcellular foams. They can consist of closed cells or open porous structures. Preliminary research into nanofoams properties has suggested significant improvements in strength and toughness over conventional and microcellular foams [3,4]. A common hypothesis predicts that nanofoams with cells smaller than the mean free path of air molecule collisions will cause the cells to behave as a vacuum. This could theoretically lead to significantly reduced thermal conductivity in appropriately structured nanofoams.

1.2 The Solid-State Foaming Process

The solid-state foaming process is the method of producing microcellular foams used in this research. It is distinguished from other foaming methods by nucleating cells in solid polymer, as opposed to polymer in a melt phase, such as during extrusion. This process consists of three steps: sorption, desorption, and foaming. In the sorption step, the solid polymer sample is exposed to high pressure gas, typically carbon dioxide (CO_2). The gas molecules diffuse into the polymer over time, until the sample is fully saturated. The saturation concentration of each polymer-gas system depends on the pressure and temperature of the gaseous environment. In

general, the saturation concentration is proportional to the pressure and inversely proportional to the temperature. The uptake of gas into the sample is observed by measuring the increasing mass of the sample over time.

During saturation, the sample is typically wrapped in a porous material, such as paper towels, to ensure even exposure to gas on all surfaces. During sorption, the gas diffuses from the surface of the sample to the core, meaning that there is a distribution of gas concentrations within the sample, with the lowest values at the core. As diffusion progresses, the concentration distribution approaches a steady state value throughout the sample. Typically, the sorption step lasts until the sample is fully saturated.

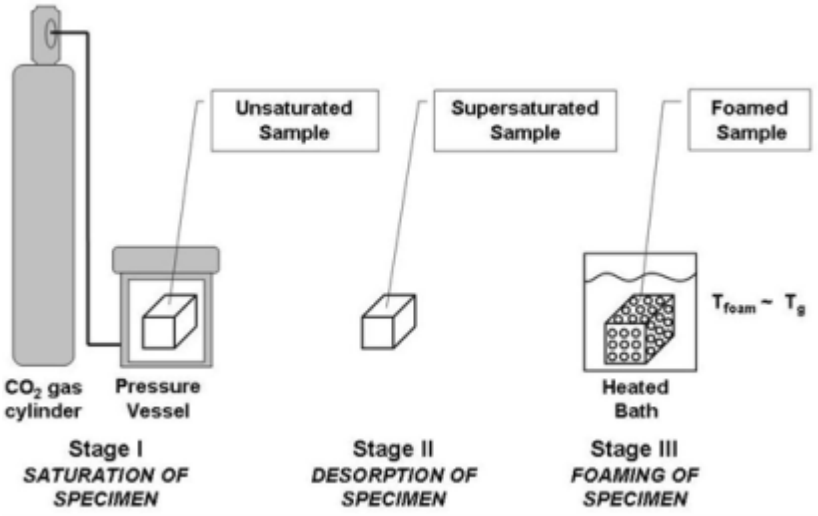

Figure 1.2: Diagram of the solid-state foaming process

In the second step, the sample is removed from the pressure and temperature controlled environment and exposed to room temperature and pressure. Under these conditions, the saturation concentration is drastically reduced, rendering the sample supersaturated. As a result, the absorbed gas diffuses back out of the solid polymer to the surrounding air. This process is referred to as desorption. Similar to sorption, desorption involves diffusion from the surface of the sample to the surroundings. Thus the gas concentration profile will be lowest at the edges and

surfaces. The extent of desorption can be controlled by the time during which it occurs and the temperature and pressure conditions that it occurs at.

The final step involves nucleating the absorbed gas into cells within the solid polymer. This is achieved by rapidly raising the temperature of the polymer sample. The rise in temperature has two effects: First, the sample becomes further supersaturated. Second, the polymer-gas system is raised above its glass transition temperature (T_g). The T_g is the temperature at which an amorphous or semi-crystalline polymer undergoes a transition from a relatively hard and brittle state to a soft and rubbery state. At a molecular level, this phenomenon can be understood as the presence of enough energy at temperatures above the T_g being present to allow the polymer chains to move in relation to one another. This polymer chain mobility allows the dissolved gas to nucleate into cells and grow, with the polymer chains rearranging themselves around the cells. The temperature that this transition occurs at depends on the polymer and the amount of gas dissolved in it. The dissolved gas acts as a plasticizer in the solid polymer, lowering the glass transition temperature. Despite the glass transition, the polymer is still considered to be in a solid state throughout the process.

This foaming step can be accomplished by a number of methods, including oil bath foaming and hot press foaming. In oil bath heating, a sample is submerged in a circulating bath of oil held at a particular temperature, called the foaming temperature. After a set amount of time, referred to as the foaming time, the sample is removed and allowed to cool in air or quenched in water. In hot press foaming, the sample is placed between the heated platens of a hydraulic compression press. The heat of the platens foams the sample while the platen clamping force compresses the sample and maintains its flatness. The sample may be released and cooled in air or cooled under pressure in the press.

1.3 Project Motivation

The traditional solid-state process described above involves sorption at room temperature and pressures of 5MPa or less. In most polymer-CO_2 systems, these conditions produce microcellular foams. However, samples saturated at high pressures and foamed at high temperatures can form nanocellular foams. Krause et al. identified a threshold concentration for the transition from closed microcellular structures to nanoporous open structures in PEI [5]. Miller et al. studied the tensile and impact properties of PEI nanofoams [4]. Most recently, Zhou et al. used supercritical CO_2 and a hot press foaming method to describe a process map for PEI nanostructures [6].

The existing research in nanocellular foams has focused on applications involving improving the mechanical properties of low density polymer foams through cell size reduction. This research represents an initial investigation into a new application for open nanoporous foams. The focus of this new application is on using the nanoporous structure as a battery separator membrane. Battery separators are permeable membranes placed between the anode and cathode of a liquid electrolyte battery. The battery separator prevents physical contact between the anode and cathode while allowing ionic transport through a liquid electrolyte. Critically, the battery separator must be very thin, porous, strong, and chemically resistant. In addition, it is desirable for the porous structure to be uniform and highly tortuous to inhibit the growth of lithium dendrites through the structure, which cause short circuits and battery failure [7].

The microcellular process is very well suited to the production of uniform, highly tortuous porous structures with pores less than 1 μm in diameter. In addition, this process can be applied to a variety of polymers with excellent thermal and mechanical properties and chemical resistance. However, two significant obstacles exist in this pursuit. First, the microcellular batch process leaves the nanoporous core locked in a solid exterior skin layer. This blocks the ionic

transport properties of the core structure. Second, the microcellular process has not been successfully employed to produce sufficiently thin nanocellular samples. Battery separators must be as thin as possible to maximize the energy density of the resulting battery. In practice, battery separators typically have a thickness of 25.4 μm (1 mil) [7].

Two potential solution paths have been identified to overcome these obstacles. First, the microcellular process may be adapted to directly produce thin porous membranes with no solid skin layer. This would involve complete elimination of desorption from the sample prior to foaming. Preliminary experiments towards this end are contained in Chapter 3. Second, a relatively thick foamed sample with solid skin may be further processed to remove the skin and reduce the thickness to the desired amount. The bulk of this research focuses on the second solution path due to its relative simplicity and expected ease of commercialization.

The first task in this endeavor is to develop a fast and reliable method for the production of nanoporous samples suitable for further research into solid skin removal. This is the primary goal of this investigation. The ideal sample should be flat and have a uniform nanoporous core free of blisters or defects.

Chapter 2 Experimental Procedures

2.1 Materials

The material used in this investigation was polyetherimide (PEI). PEI is an amorphous thermoplastic with excellent mechanical strength and chemical resistance. Critically, the mechanical properties of PEI are stable and predictable up to 200°C. PEI has a glass transition temperature of 217°C and a density of 1.27 g/cm^3. PEI resin is translucent amber in color and turns white when foamed, as seen in Figure 2.1. The PEI used in this investigation was SABIC brand Ultem 1000. The material was obtained from McMaster-Carr as 0.040" (1.016 mm) sheets. The PEI sheets came with a protective film on the top and bottom surfaces. This film was removed prior to processing the samples.

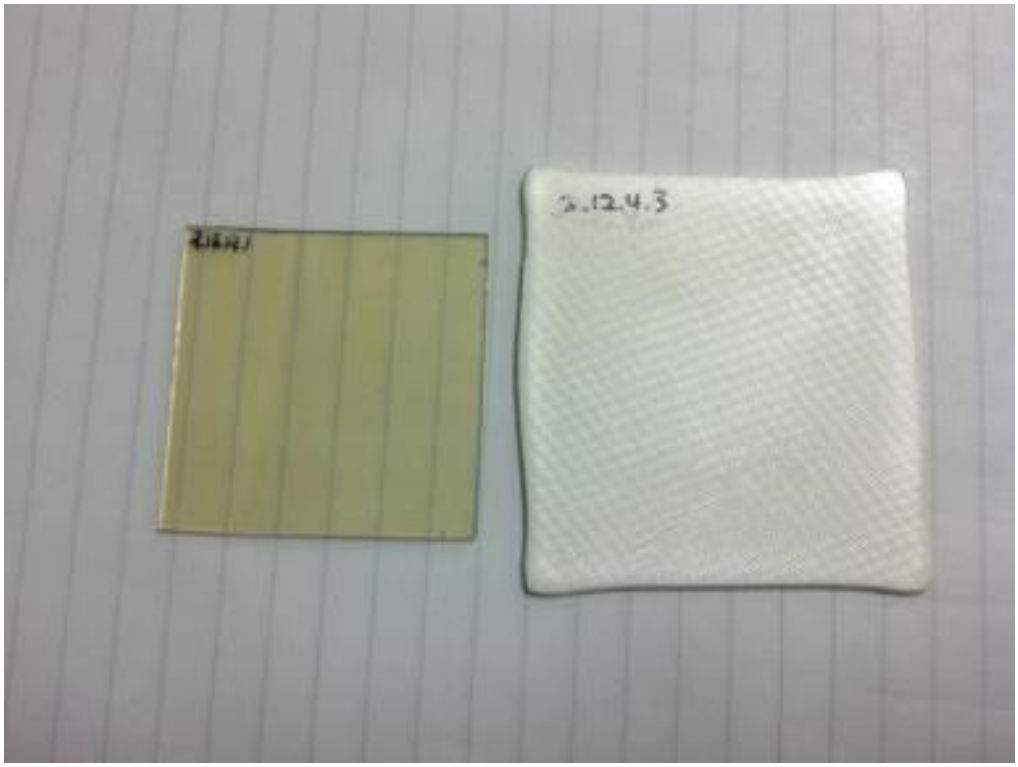

Figure 2.1: PEI samples before (left) and after (right) foaming.

2.2 Sample Preparation

The thick PEI sheet cannot be reliably cut using scissors, so a foot-operated shear was used instead to cut samples into 1.016 x 45 x 45 mm squares. Other cutting methods were experimented with, including hand shears and a band saw. The band saw led to significant cracking of the edges of the samples. Both methods of shearing leave a crimped edge on the sample. Preliminary experiments were conducted to compare the foaming of samples with this crimped edge intact to those where the edge had been filed down flat. No difference in foaming results was noticed, so the filing step was not employed in further experiments. All samples were inspected for flaws and cracks and uniquely labeled prior to experimentation. Samples were not dried prior to performing these experiments.

2.3 Saturation Method

2.3.1 Introduction

The first step in the microcellular process involves the saturation of the solid polymer sample with gas at elevated pressure. All samples were saturated with 99.9% pure CO_2 from cylinders supplied by Praxair. The saturation pressure, temperature, and time were varied to control the resulting gas concentration of each sample. In all cases, the samples are individually wrapped in paper towel before saturation to ensure even exposure to the gas.

2.3.2 Supercritical CO_2 Saturation Apparatus

The supercritical CO_2 saturation apparatus was employed for saturation experiments in this research. Figure 2.2 shows the main components of the supercritical CO_2 system. This system consists of a high-pressure steel pressure vessel connected to a Teledyne Republic/Sprague S-86-

JN gas booster. The gas booster uses compressed air to drive a pump that pressurizes the vessel above the cylinder CO_2 pressure. The compressed air pressure is controlled by an Omega CN8500 process controller with a resolution of 0.01 MPa. The pressure vessel also has an external heating pad controlled by a Cole-Parmer Digi-Sense 89000-00 temperature controller unit. This unit uses a thermocouple located on the inside of the vessel to monitor the saturation temperature. This apparatus was used for saturating samples at 20 MPa and 45 °C.

Figure 2.2: Supercritical CO_2 saturation apparatus.

2.3.3 Gas Concentration Measurement

The extent of gas uptake in the polymer is measured by comparing the change in mass. Mass measurements are performed on a METTLER AE240 balance with an accuracy of 10 μg. In order to measure the concentration of gas in the sample during sorption, the sample must be removed from the pressure vessel and measured on the balance at ambient pressure. During this time, gas will desorb from the sample. This contributes to the error in gas concentration

measurement. The longer the sample desorbs before measuring the concentration, the more error will be introduced. Larger samples will lose a smaller percentage of the total dissolved gas and thus exhibit less error in concentration measurement. Small or very thin samples with a high surface area to mass ratio can show significant errors in concentration measurement. After measurement, the samples are returned to the pressure vessel and again exposed to high pressure. In this investigation, the gas concentration in the sample is reported as a mass percent by the following equation.

$$C = \frac{m - m_{initial}}{m_{initial}} \times 100 \tag{2.1}$$

2.4 Foaming Method

2.4.1 Introduction

Once a sample has been saturated with CO_2, a heating step is employed to nucleate the dissolved gas into cells. Several methods of introducing heat to saturated samples were used in this work. Oil bath foaming provides a fast and controllable heat source but is limited by temperature constraints and produces curved samples. Press foaming is comparatively complicated but produces flat, evenly foamed samples.

2.4.2 Press Foaming

A hot press foaming method was developed to allow for the creation of flat foamed samples. The press foaming technique was first developed by Nadella et al. to produce large flat samples [8]. Miller further refined the process, adding a porous fabric layer between the sample and the platens and ceasing the use of metal shims between the platens [9].

Saturated samples were foamed in a Wabash Genesis hydraulic press. This press is capable of temperatures up to 343°C (650°F) and clamping forces between 0.89 and 444.8 kN (0.1 and 50.0 tons). The hydraulic press uses Imperial units as input for the clamping force, so further mention of this parameter in this report will be in tons. After saturation, the samples were desorbed at room temperature and pressure for a set amount of time. One sample at a time was placed in the middle of the hot press platens, which have been preheated to the desired foaming temperature. The samples were held between four layers of PTFE-coated fiberglass fabric. The top and bottom layers of fabric are tightly woven fiberglass intended to allow for easy sample release from the platens. The layers immediately adjacent to the sample have a porous, open weaving that allows for excess CO_2 from the sample to be released during foaming. This reduces the formation of surface blisters on the sample during foaming. The hot press is set to close rapidly until it reaches an adjustable point, set to be just thicker than the unfoamed sample. At this point it closes slowly on the sample and raises the pressure up to a set point. It maintains this pressure and temperature for a set foaming time, after which the platens open and the sample is promptly removed. The sample is cooled at room temperature.

Figure 2.3: Wabash hot press.

2.5 Characterization Method

2.5.1 Introduction

The primary means of sample characterization used in these experiments were relative density measurement by displacement and microstructure characterization by scanning electron microscopy. Thus a foam sample can be described by its ratio of polymer to voids and the size and nature of these voids.

2.5.2 Density

The density of each sample was determined according to ASTM standard D792. This method involved comparing the mass of the sample in air to its mass while suspended in a fluid. In all measurements, distilled water was used as the working fluid. The sample mass was first measured in its dry state three times to ensure consistency. The sample was then submerged in

water, placed against the measurement apparatus, and the mass was measured again. This was repeated a total of three times for each sample. Care was taken to ensure that minimal air bubbles were adhered to the surface of the sample upon insertion into the water. Air bubbles attached to the sample surface add buoyancy to the sample, thus introducing error to the final measurement. The sample density in this investigation is reported as a relative density compared to that of solid PEI (1.27 g/cm^3).

Figure 2.4: Balance with density measuring apparatus.

2.5.3 Electron Microscopy

Microstructure characterization was performed by analyzing Scanning Electron Microscope (SEM) images of the microstructure of the foams. SEM samples were first prepared by liquid nitrogen freeze fracture. Samples were cut to a manageable size and notched at the desired fracture plane using a razor blade. The samples were then submerged in liquid nitrogen for at least one minute. Immediately after removal from the nitrogen, the samples were pulled apart at the fracture surface using pliers.

The PEI samples used in this investigation showed anisotropic fracture behavior. Samples fractured along one direction showed jagged and curved fracture surfaces unsuitable for imaging. However, samples fractured using the same method but in the orthogonal direction showed flat and clean fracture surfaces ideal for imaging. This effect is likely due to anisotropic material properties caused by the extrusion process used to form the PEI sheets.

Fractured samples were mounted in vertical sample holders with carbon tape connecting the fracture surface to the metal holder for charge dissipation purposes. The mounted samples were sputter coated with Au/Pd for 60 seconds using an SPI Sputter Module Controller. An FEI Sirion SEM was used to obtain images of the fracture surface. Low magnification images (< 10000x) were collected using the default high resolution detector with an accelerating voltage of 5 kV, a spot size of 3, and a working distance around 5 mm. Higher magnification images require the use of the ultra-high resolution detector at an accelerating voltage of 20 kV. The high resolution detector provides much clearer and higher contrast images of the sample nanostructure.

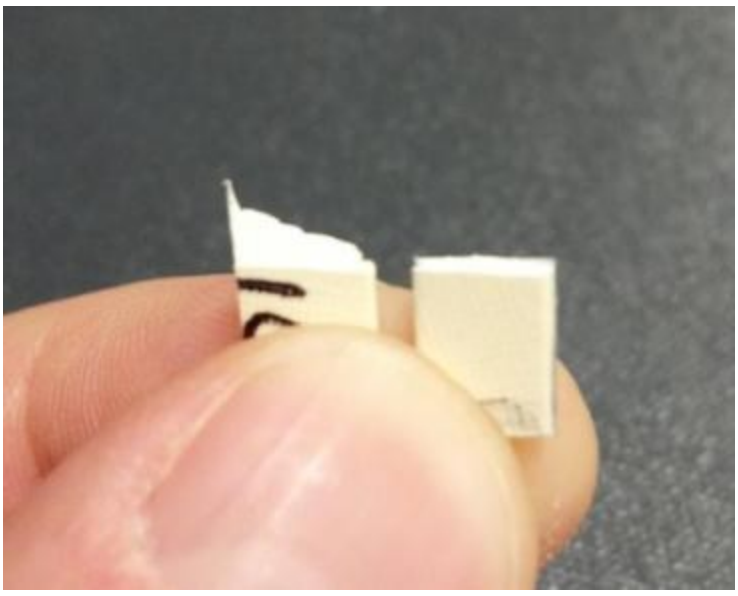

Figure 2.5: Fracture surfaces cut from the same sample but fractured in orthogonal directions. The left surface is jagged and cannot be imaged properly in the SEM. The right surface is flat and ideal for SEM imaging.

2.5.4 SEM Image Analysis

The SEM images were characterized by skin thickness, transition layer thickness, and cell size. A cross-section of a typical foamed sample, such as that shown in Figure 2.6, shows a core of nanoscale cellular structure with transition layers of micro-scale cells on the top and bottom, followed by a thin solid skin. These features are caused by locally reduced gas concentrations at the edges of the sample due to desorption. Skin thickness was measured by drawing ten lines perpendicular to the skin surface at even intervals along the image. The skin thickness is defined as the average distance along each line to the first cell encountered. The same procedure was used to estimate the thickness of the transition layer, though the interface between the transition layer and the nanocellular core is less distinct.

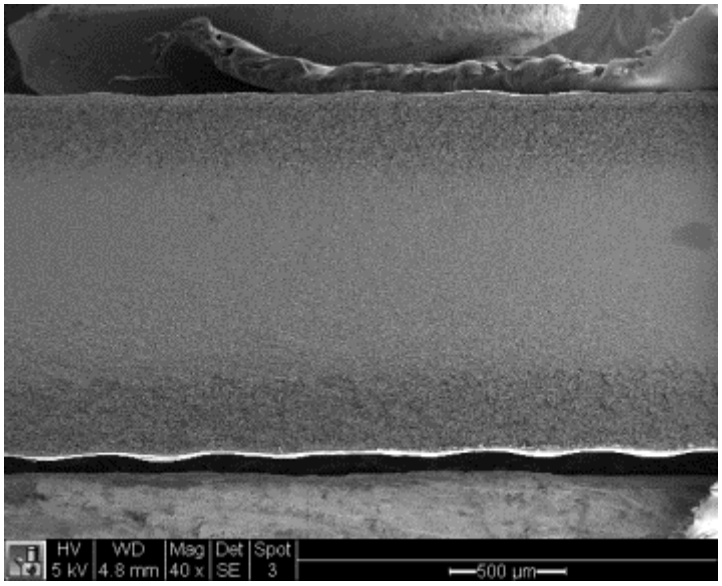

Figure 2.6: Typical foamed sample cross-section. The nanocellular core is contained between the darker transition layers and the solid skin layer at the edges.

Cell size measurement in nanoporous foams presents a significant challenge. Microcellular foams contain roughly spherical voids with distinct edges. By contrast, nanocellular foams consist of an interconnected network of voids with no clearly measurable cells. A reported cell size is actually best described as the characteristic length of the nanoscale features. This number

is highly dependent on the morphology of the nanostructure. Small changes in the processing parameters result in significant changes in nanostructure that makes objective cell size measurement difficult.

For this investigation, the cell size was measured using ImageJ, which is free software available from the National Institutes of Health. Cell size was measured as follows: First, the image is loaded into ImageJ and the scale is calibrated. Next, a grid is drawn on the image using the grid plugin. The grid makes it easier to avoid repeat measurements of cells. Then, the freehand selection tool is used to trace the outline of the selected cell and measure the area of the resulting selection. In order to convert this area into a linear dimension, the cell is assumed to be spherical with the measured area representing the mid-plane of the sphere. Thus, the N measured areas are converted to characteristic diameters and averaged by the following equation:

$$\mathrm{d} = \frac{\sum_{i=1}^{N} 2\sqrt{\frac{A_i}{\pi}}}{N} \tag{2.2}$$

This measured average cell size depends heavily on the criteria for cell selection. Figure 2.7 shows a typical sample at high magnification. For this investigation, a feature was considered a cell if it was darker than its surroundings, had a distinct edge, and did not contain smaller features that also fit these criteria. Thus, only the smallest features are included in the measurement.

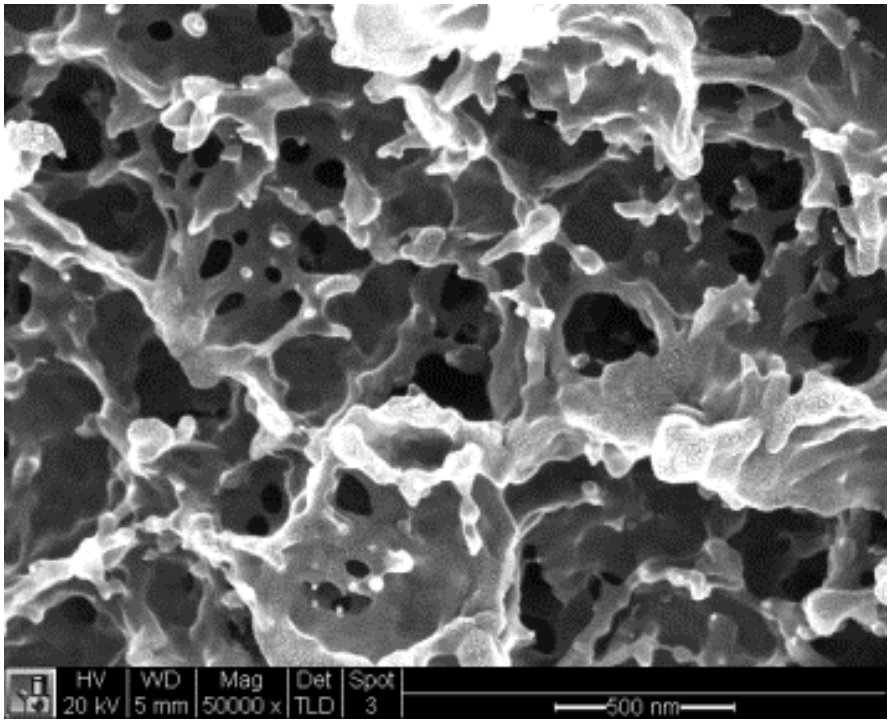

Figure 2.7: Nanocellular features in a typical sample.

Chapter 3 Preliminary Experiments in Thin Film Foaming

3.1 Introduction

This experiment was performed as a preliminary attempt to produce thin nanocellular films using a variation of the microcellular batch process. This represents an alternative solution path to the production of battery separators. Specifically, the goal was to study the feasibility of foaming thin polymer films with little or no solid skin layer. The microcellular batch process is difficult to apply to thin films because of their susceptibility to desorption. Due to the short diffusion length scale, a thin film sample will desorb much faster than a thicker sample.

Previous work by Romano Montecillo in the Microcellular Plastics Laboratory attempted to eliminate desorption from the microcellular process by foaming the sample while still at the saturation pressure [10]. This was accomplished by heating the pressure vessel with the saturated sample inside, still at the saturation pressure. Unfortunately, the long heating times used in this process lead to significant desorption during heating, causing the formation of thick skin layers.

This experiment was performed on a novel apparatus designed to increase the heating rate by placing ceramic heating elements inside the pressure vessel. The hypothesis was that if the heating rate could be increased enough, the desorption time would be significantly reduced, resulting in foamed thin films with little or no solid skin. The apparatus was built by a student team consisting of Matt Christie, Zach Glaser, Nat Mottaz, and Dylan Turner in the spring of 2011.

3.2 Experimental Method

The in situ foaming apparatus consists of a steel pressure vessel with circular ceramic heating elements positioned on an adjustable frame inside the vessel, as seen in Figure 3.1. The sample is held between two thin metal screens positioned on an adjustable platform sandwiched between the two heaters. Both the distance between the heaters and the position of the sample can be adjusted. The pressure vessel is supplied with CO_2 by a pressurized cylinder controlled by an Omega process controller with a resolution of 0.01 MPa. The sample saturation process occurred at room temperature.

This experiment was performed using Ultem brand PEI film supplied by McMaster-Carr. The film thickness was 0.127 mm (0.005”). Previous experiments by John Lu in the Microcellular Plastics Laboratory identified a necessary saturation time of 45 minutes for 0.076 mm PEI samples at a pressure of 5 MPa [11]. Experiments with the slightly thicker samples used in this experiment showed that saturation was achieved after 60 minutes at 5 MPa.

After the saturation step, the samples were foamed in situ by the internal heaters. The heating elements are ceramic disks 3.25” in diameter and 11/32” thick. They have a maximum power output of 400 W each at 120 VAC, with a maximum temperature of 400°C. The heaters are connected through a pressure rated feed-through fitting in the side of the pressure vessel to a 120 VAC power outlet. As the temperature in the pressure vessel rises, the pressure increases correspondingly, in accordance with thermodynamic principles. The pressure controller used in this experiment was set to allow this pressure increase without the overpressure venting traditionally employed in saturation experiments. After a set foaming time, during which the heaters are powered, the heaters are disengaged and the vessel is allowed to cool down to room temperature before the pressure is released and the sample is removed.

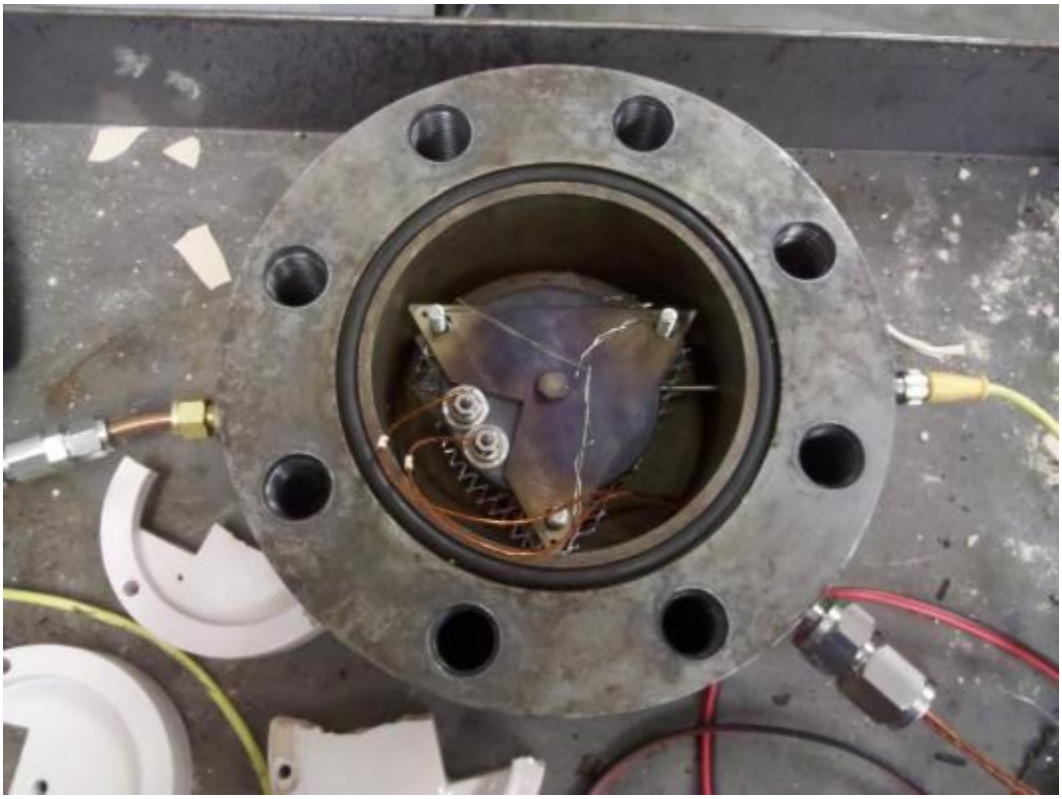

Figure 3.1: The interior of the in situ pressure vessel apparatus.

3.3 Results

Preliminary foaming experiments with the heaters positioned 4.5 mm above and below the sample did not result in foaming. Further experiments with the heaters placed as close as possible (<1 mm) to the sample and heating times between 1 and 2 minutes did succeed in producing foam. These samples foamed very unevenly, as seen in Figure 3.2. The presence of the metal mesh caused some regions to be blocked from the heaters, revealing the pattern of the mesh on some samples. Samples that foamed for longer times also had significant surface blistering. SEM imaging of the foamed samples reveal micro-scale cells and large solid skin layers, as seen in Figure 3.3.

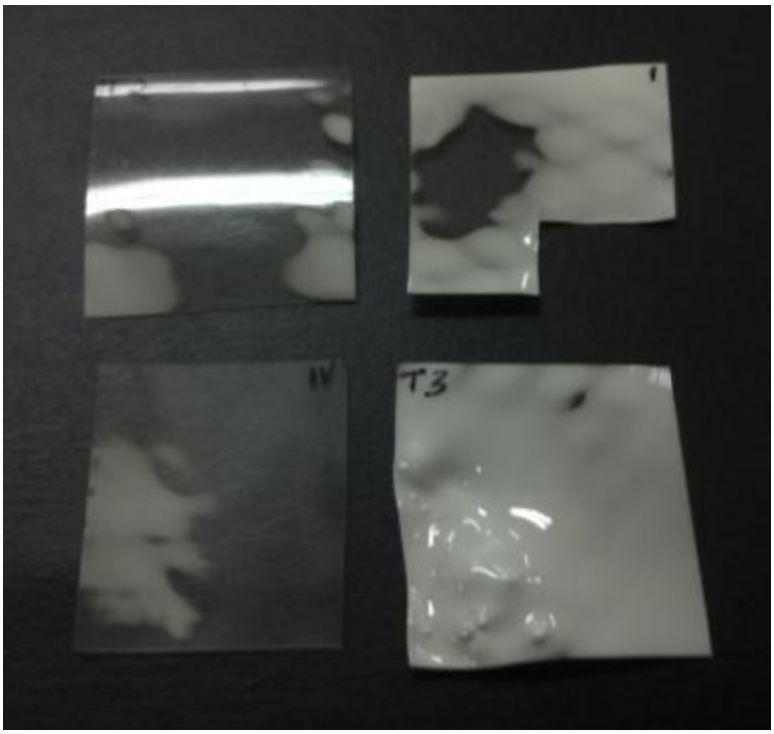

Figure 3.2: PEI films foamed in the in situ foaming apparatus. These samples show foamed (opaque) and unfoamed (translucent) regions as well as blistering.

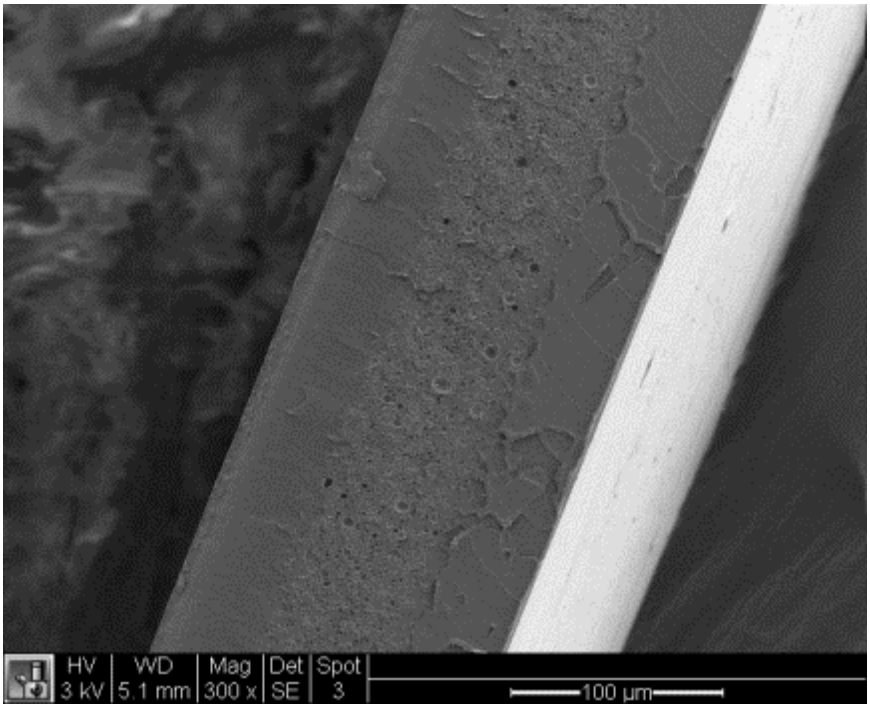

Figure 3.3: PEI film foamed in the in situ foaming apparatus. This sample was saturated at 5 MPa and foamed for 60 seconds.

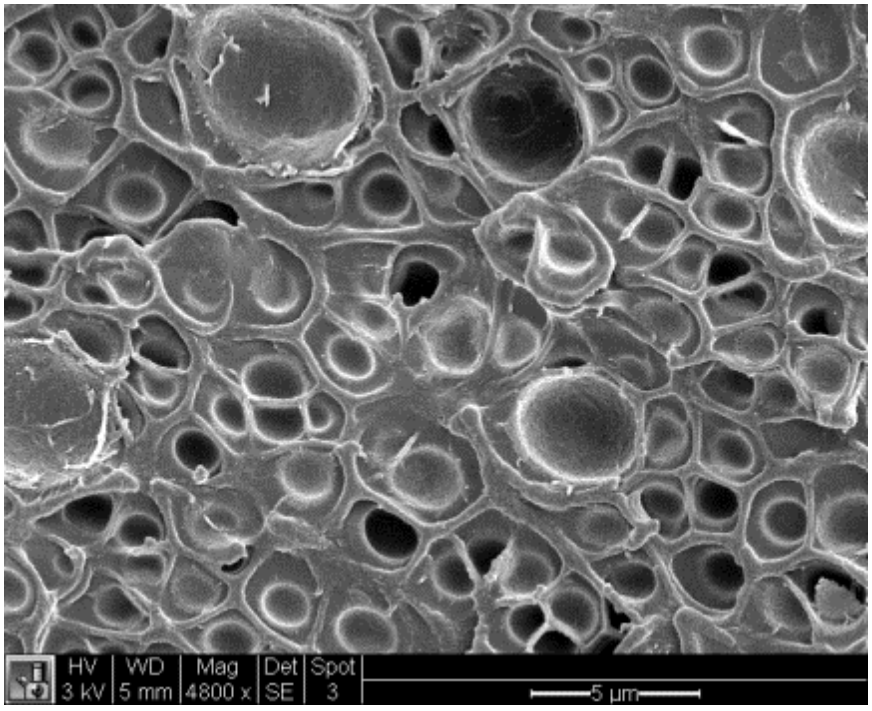

Figure 3.4: Microstructure of an in situ foamed PEI film.

3.4 Discussion

The results of preliminary experiments with the in situ foaming apparatus show that while foaming of thin films is possible with this method, the solid skin layer has not been eliminated or significantly reduced in the process. Furthermore, the foamed samples did not show open nanocellular structures. The presence of the solid skin layer is likely due to desorption from the surfaces of the sample that occurs while the sample is heating but prior to reaching the threshold foaming temperature. Though the saturation pressure is still present, the increased temperature reduces the solubility of gas in the polymer, leading to desorption.

Further refinements of this apparatus may succeed in more satisfactory foaming of thin polymer films. The heating rate of the ceramic elements is not sufficient to effectively eliminate desorption from the process. Improvements in the heating rate through the use of better heaters or other heating methods may produce better results. However, for the purposes of this

investigation, the preliminary results with this method were not promising enough to warrant further experiments.

Chapter 4 PEI - Supercritical CO_2 Characterization

4.1 Introduction

The microcellular process relies upon an in depth understanding of the polymer-CO_2 system. Previous research in the Microcellular Plastics Laboratory has characterized the absorption and desorption of CO_2 by PEI under pressures less than or equal to 5 MPa at room temperature. This chapter establishes the CO_2 absorption and desorption behavior of PEI at 20 MPa and 45°C. Under these conditions, the gas inside the pressure vessel is a supercritical fluid. The results of this guide the saturation time used in further experiments.

These saturating conditions were chosen in an effort to minimize the necessary saturation time, but are constrained by safety and reliability concerns. Higher pressures lead to higher saturation concentrations but longer saturation times. The gas booster pump has a limited maximum pressure that depends on the pressure of the shop air and the pressure of the connected gas tank. Particularly when many measurements are being taken for sorption experiments, the amount of gas vented at these higher pressures depletes gas tanks rapidly. This requires careful planning to ensure constant availability of full tanks. In addition, the gas booster pump has been reported to have o-ring problems at higher pressures. Thus, a moderate pressure of 20 MPa was chosen.

The temperature of the pressure vessel must be held above the critical point of CO_2 (31.1°C and 7.38 MPa) to ensure that the gas is a supercritical fluid. Higher saturation temperatures lead to faster diffusion, but decrease the saturation concentration. In addition, there are significant safety concerns involved with temperatures capable of causing burns or igniting surrounding

objects. A saturation temperature of 45°C was chosen to provide fast saturation without compromising safety.

4.2 Experiment

In the sorption study, two samples were saturated separately using the supercritical pressure vessel system. The samples were removed periodically and the gas concentration was measured by comparing the mass to the original value. There is more error introduced in sorption measurements taken from samples in the supercritical pressure vessel because of the longer venting time and sample removal time required. In addition, after each measurement, the pressure vessel takes longer to pump back up to a steady saturation pressure than pressure vessels that do not use a gas booster. The total time elapsed between beginning to vent the vessel and returning to a steady state saturation temperature can be as much as 15 minutes. Thus, each measurement has a significant effect on the sorption behavior. For these reasons, fewer measurements were taken than in typical sorption experiments.

The desorption study consisted of measuring the mass of a saturated sample over time as gas desorbed out. The sample was saturated for 5 days prior to removal from the pressure vessel. Once removed, the sample was allowed to sit at room temperature and pressure on a piece of paper towel to ensure even desorption from all surfaces. The mass of the sample was periodically measured over the next 20.5 hours.

4.3 Results

Figure 4.1 shows the results of the sorption experiments. Sample 1 reached a maximum concentration of 11.4% and sample 2 reached a maximum of 10.9%. The difference between the

two can be attributed to different elapsed desorption times between pressure release and measurement. For future experiments, the samples are considered to be saturated after 72 hours of sorption.

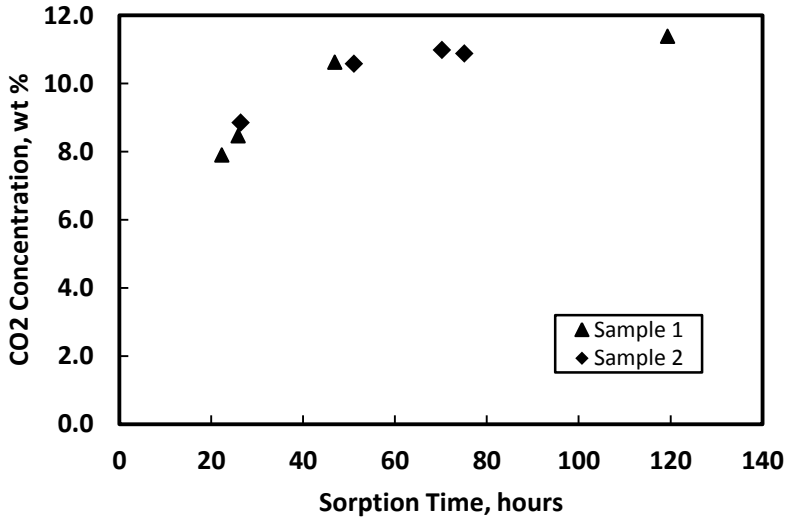

Figure 4.1: Sorption results.

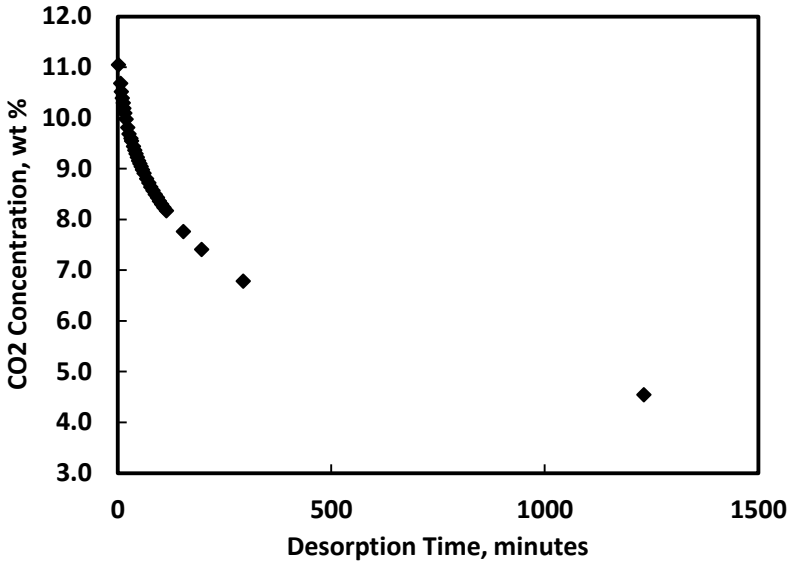

Figure 4.2: Desorption results.

Figure 4.2 contains the results of the desorption experiment. The rapid initial rate of desorption causes a significant drop in concentration before the first measurement, contributing to the error in the sorption experiment.

4.4 Discussion

The sorption experiment established the necessary saturation time used in all further experiments. This time, 72 hours, is considered a minimum amount sufficient for a sample to be considered saturated. The gas concentration of the sample is assumed to not change from this condition with longer saturation times. The saturation times of the remainder of the experiments described in this thesis are mostly longer than 72 hours, due to logistical factors.

Chapter 5 Desorption Study

5.1 Introduction

The first experiment focused on varying the desorption time prior to foaming. Preliminary experiments suggested a significantly higher rate of internal blistering at lower desorption times. The internal blisters form around the mid-plane of the plastic sheet and expand perpendicularly to the clamping force, as seen in Figure 5.1. In extreme cases, the internal blisters can join and form large air pockets in the sample, as seen in Figure 5.2. Samples showing these features after foaming often crack audibly while in the hot press. For the purposes of this research, these blisters are considered to be undesirable. The goal of this experiment was to determine whether increased desorption time prior to foaming could reduce the incidence of internal blistering.

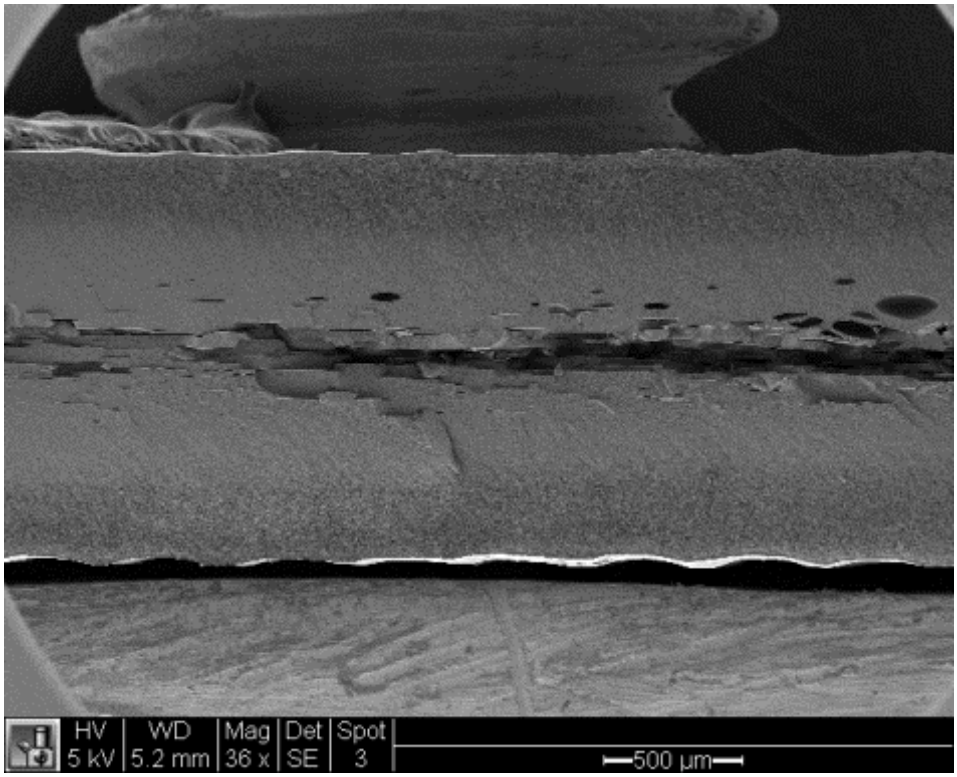

Figure 5.1: Mid-plane blistering in a press foamed sample. This sample was desorbed for 25 minutes prior to foaming for 3 minutes at 195°C and

a clamping force of 0.5 tons. The clamping force of the hot press during foaming was in the vertical direction in this image.

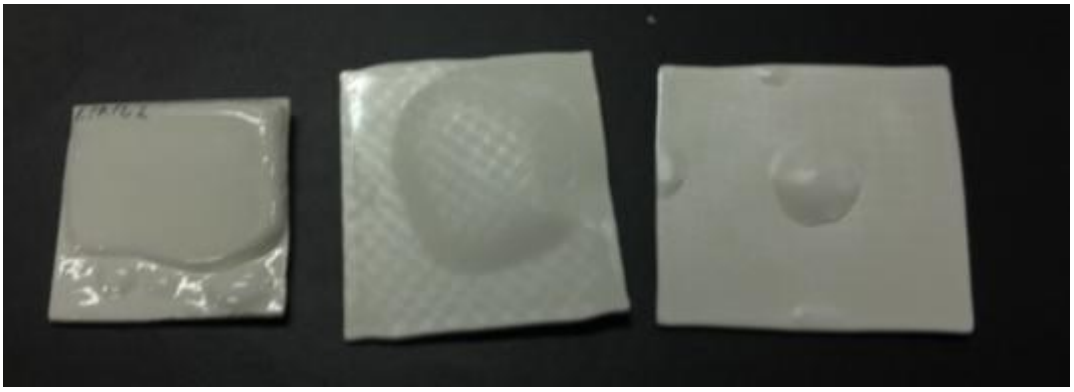

Figure 5.2: Samples showing evidence of significant internal blistering.

5.2 Experiment

One sample was foamed at each of eight desorption times. The chosen desorption times were every ten minutes from 5 to 75 minutes. All samples were foamed for 3 minutes at a platen temperature of 195°C and a clamping force of 0.5 tons. The resulting foam samples were characterized by the presence of internal blisters, relative density, skin layer thickness, and transition layer thickness.

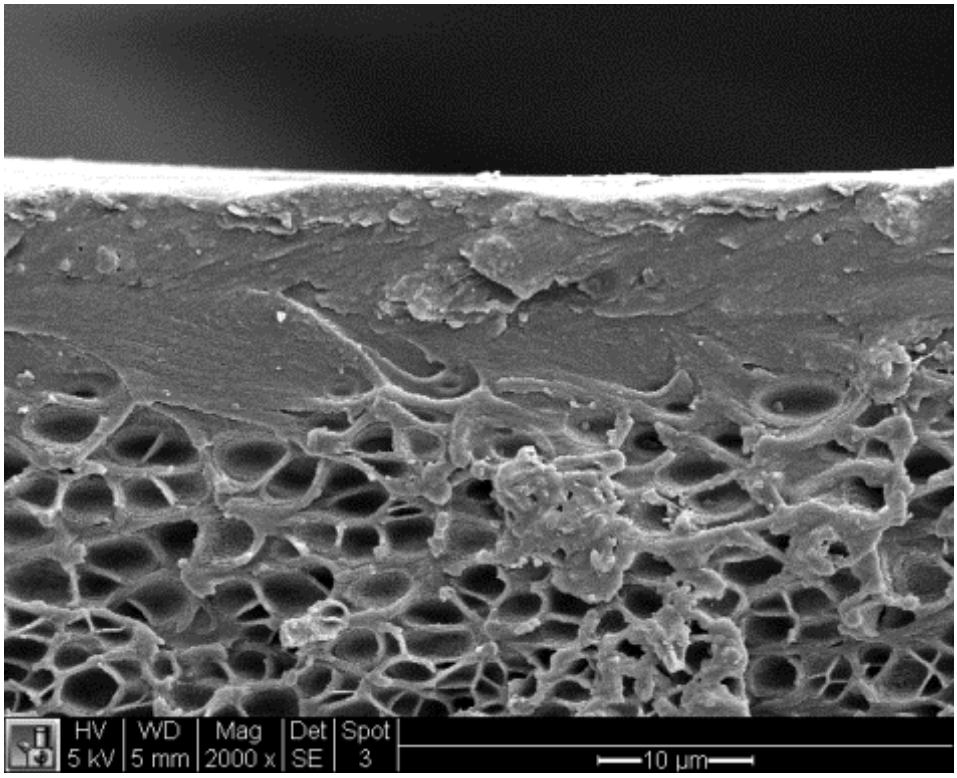

Figure 5.3: The solid skin layer of a desorption study sample. The cells immediately adjacent to the skin layer are microcellular transition layer cells.

5.3 Results

Figure 5.4 shows the results of varying desorption time prior to foaming the sample in the press. The solid skin remains between 10-20 μm thick, while the transition layer grows steadily from 54 to 326 μm. This effect is due to the diffusion of CO_2 out of the sample during desorption. The gas escapes at the surface of the sample, where the lowest concentrations are found. The concentration increases steadily from here to the core region, which remains at its saturation concentration. The locally lower gas concentration near the surface leads to the development of fewer and larger cells characteristic of the transition layer. Thus, more desorption leads to a thicker transition layer. All samples foamed after less than 35 minutes of

desorption contained considerable internal blistering. Samples foamed after 35 or more minutes contained no internal blisters but had thicker transition layers.

Table 5.1: Desorption Study Results

Sample	Desorption Time, m	Blistered?	Curved?	Mean Thickness, mm	Relative Density	Skin Thickness, µm	Transition Layer Thickness, µm
4.26.1.1	5	Y	N	1.34	55.4	10	54
4.26.1.2	15	Y	N	1.48	46.0	14	106
4.26.1.3	25	Y	N	1.51	45.3	15	243
4.26.1.4	35	N	N	1.56	44.1	17	208
4.26.1.5	45	N	N	1.55	46.9	15	210
4.26.1.6	55	N	N	1.59	44.0	20	284
4.26.1.7	65	N	N	1.56	44.0	18	309
4.26.1.8	75	N	N	1.60	40.5	17	326

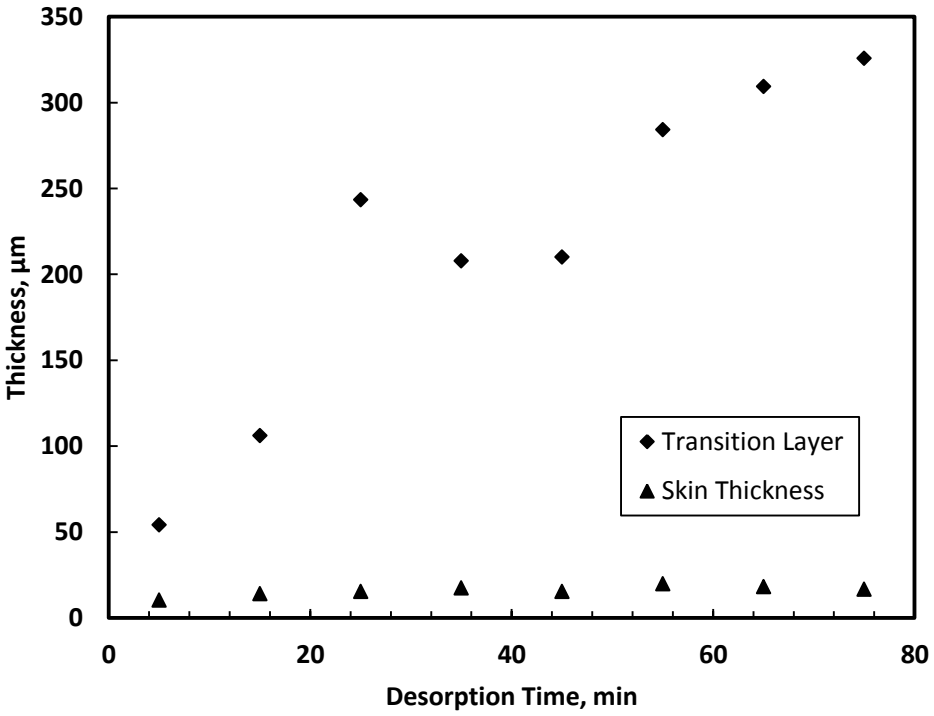

Figure 5.4: Transition layer and skin thickness results as a function of desorption time.

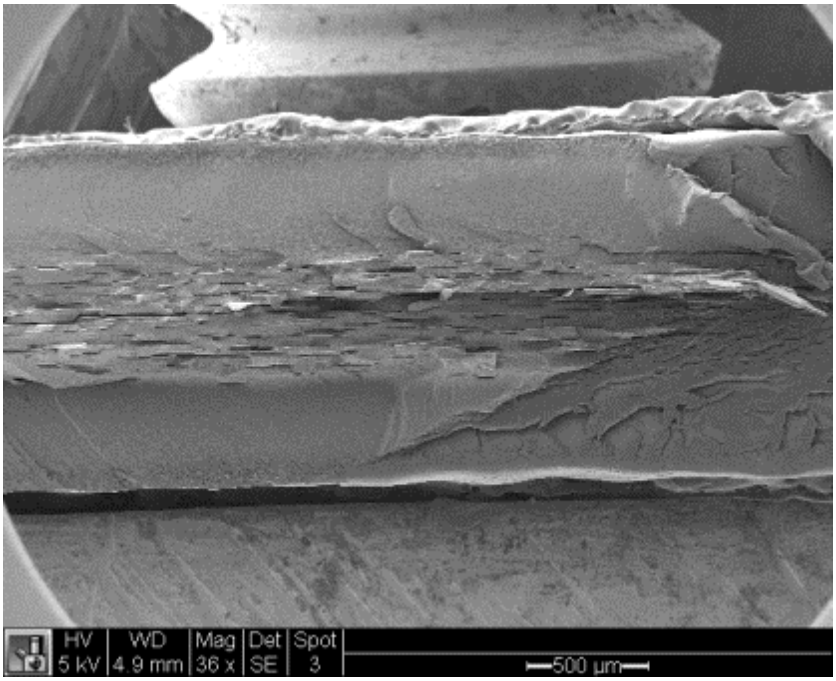

Figure 5.5: Sample 4.23.1.2 cross-section showing relatively thin transition layer and internal blistering. This sample desorbed for 15 minutes.

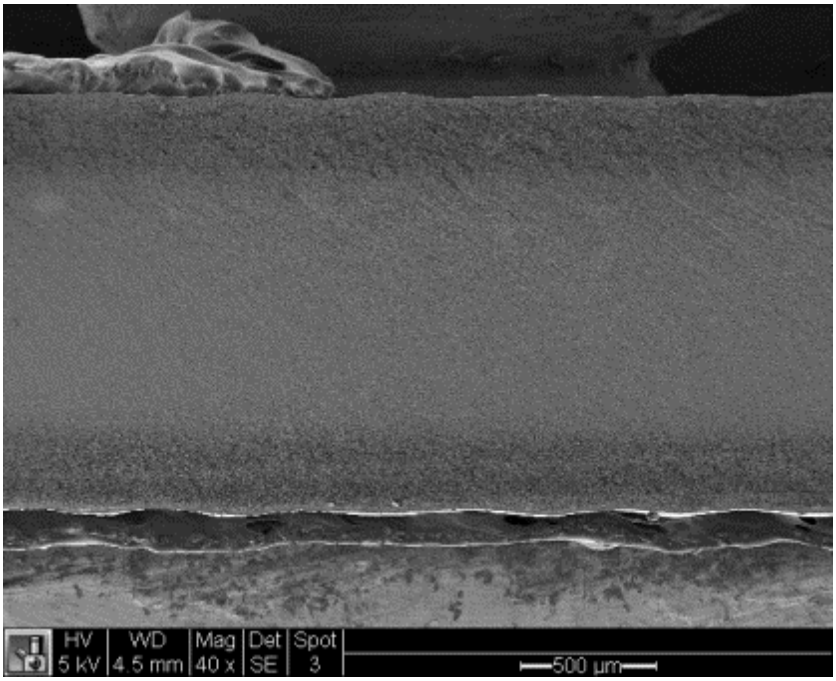

Figure 5.6: Sample 4.23.1.7 cross-section showing relatively thick transition layer and no internal blistering. This sample desorbed for 65 minutes.

5.4 Discussion

The desorption study found that internal blistering during press foaming can be avoided with longer desorption times. Critically, the necessary desorption time for avoiding internal blistering is short enough that the resulting sample will still possess a nanocellular core region. Under these conditions, samples foamed after at least 35 minutes of desorption did not contain internal blisters. The mechanism of this effect is not fully understood. However, the formation of large, connected blisters is likely due to adherence between the platens and the surface of the samples. Despite using the PTFE-coated fabric to prevent the sample from adhering to the platen, some degree of attachment remains, often causing the sample to stick to the upper platen when the press opens. The tension forces caused by this attachment likely are responsible for pulling apart the blister-weakened halves of the foamed samples.

Measurements showed that the skin thickness did not increase steadily with desorption time. The skin thickness remained between 10 and 20 μm. By contrast, the transition layer thickness increased with desorption time from 54 to 326 μm. The transition layer thickness is a critical parameter in further processing of these samples for skin and transition layer removal. A thicker transition layer means more material must be removed to expose the nanoporous core.

Chapter 6 Foaming Time Study

6.1 Introduction

This experiment focused on investigating the effect of varying the foaming time. This is measured as the duration that the press holds the sample during foaming. Preliminary experiments showed that samples held in the press for very short amounts of time (< 30 seconds) would foam but would have significant curvature after release from the press. A primary goal of this investigation is the production of flat samples for further processing. Longer foaming times were hypothesized as a method of reducing curvature by relaxing residual stresses caused by foaming.

In traditional microcellular foaming, longer foaming times are associated with larger cells, as nucleated cells grow by absorbing CO_2 from the surrounding polymer matrix. This phenomenon is well characterized and explained by classical nucleation and growth processes. This experiment attempted to observe the same phenomenon in nanocellular press foaming to further characterize the process.

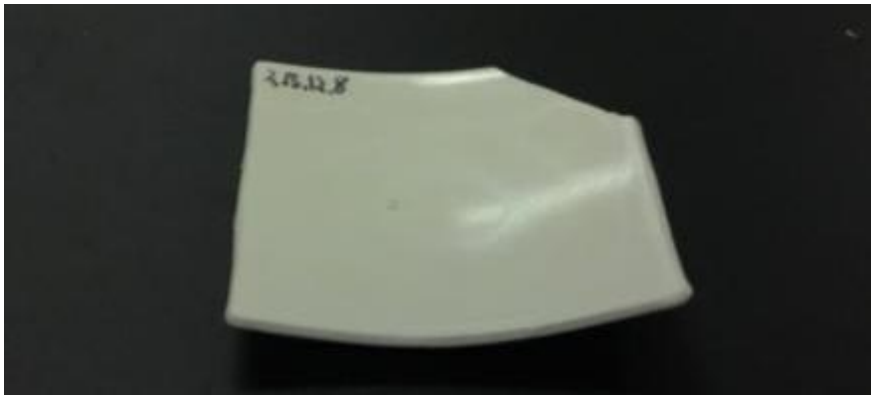

Figure 6.1: Preliminary experiment sample showing significant curvature after foaming for 1 minute at 195°C.

6.2 Experiment

The foaming times selected for this study were 0.5, 1, 1.5, 2, 2.5, 3, 3.5, 4, 4.5, 5, 7.5, and 10 minutes. One sample was foamed for each selected foaming time. The clamp force was set to 0.5 tons and the platens were heated to 195°C. Due to the long foaming times necessary, the samples were allowed to desorb for 60 minutes before being placed in a freezer set to 0°C to retard further desorption. The samples were then removed two at a time and promptly foamed. The goal was to minimize the difference in desorption between all of the samples.

6.3 Results

This experiment showed that samples foamed under these conditions for 3 minutes or longer were not curved. Table 6.1 contains the results for each sample. Figure 6.2 shows the difference in curvature between two of the samples.

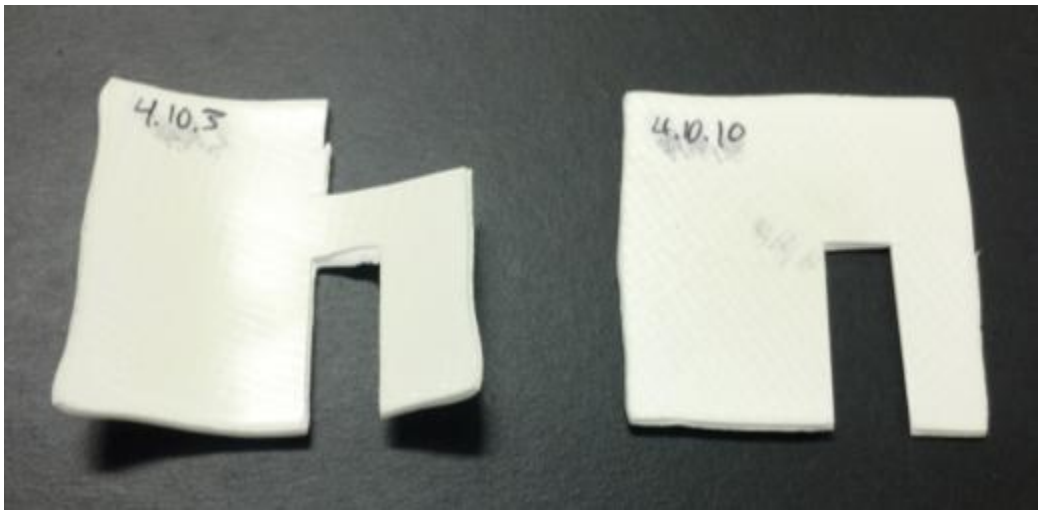

Figure 6.2: Samples foamed for 1.5 minutes (left) and 5 minutes (right). The curvature is apparent in the shorter foaming time sample. Rectangular cutouts are the result of taking samples for density measurement and electron microscopy.

Table 6.1: Foaming time experiment results.

Sample	Foam Time, min	Curved?	Mean Thickness, mm	Relative Density	SEM Analysis	
					Average Cell Size, nm	Cell Size Standard Deviation, nm
4.10.1	0.5	Y	1.79	36.4%	51	26
4.10.2	1	Y	1.73	40.0%	51	26
4.10.3	1.5	Y	1.62	41.2%	62	29
4.10.4	2	Y	1.56	42.5%	67	37
4.10.5	2.5	Y	1.62	43.6%	72	42
4.10.6	3	N	1.46	48.2%	62	32
4.10.7	3.5	N	1.37	52.8%	67	57
4.10.8	4	N	1.44	52.1%	90	54
4.10.9	4.5	N	1.40	54.0%	99	65
4.10.10	5	N	1.47	51.2%	94	62
4.10.11	7.5	N	1.46	53.4%	97	51
4.10.12	10	N	1.39	54.2%	68	55

The results of this experiment show that increased foaming time can result in flat samples. However, increasing the foaming time also has a significant effect on the nanostructure of the foam. Figure 6.3 shows the average cell size as a function of foaming time. There is a clear trend of cell growth with increased foaming time for samples foamed for less than 5 minutes. Figure 6.4 shows a similar trend of growing relative density in samples foamed for less than 5 minutes.

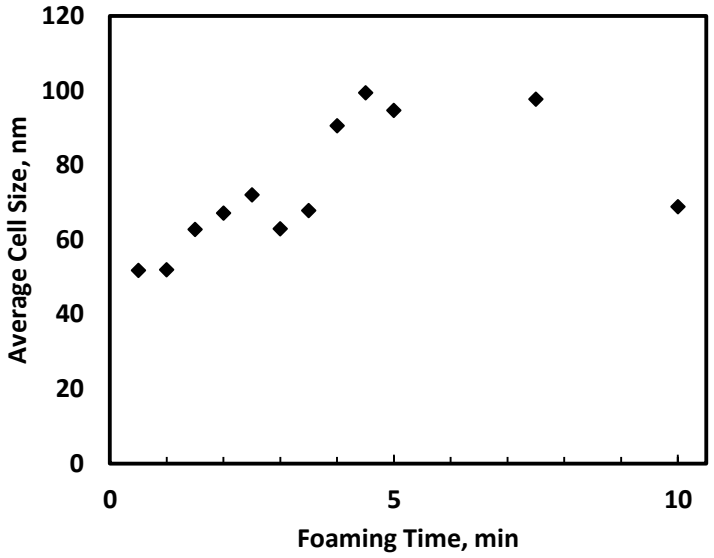

Figure 6.3: Foaming time experiment results. The average cell size is presented as a function of the foaming time. All samples were foamed at 195°C with a clamping force of .5 tons.

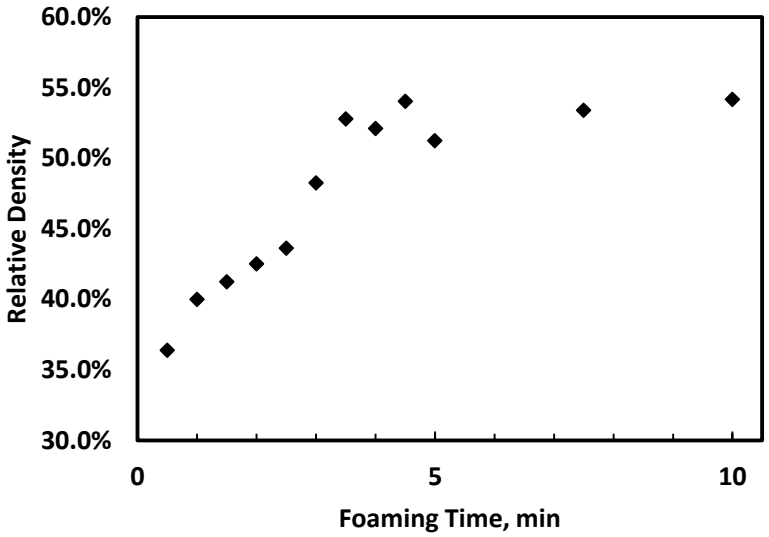

Figure 6.4: Foaming time experiment results. The relative density is presented as a function of the foaming time. All samples were foamed at 195°C with a clamping force of .5 tons.

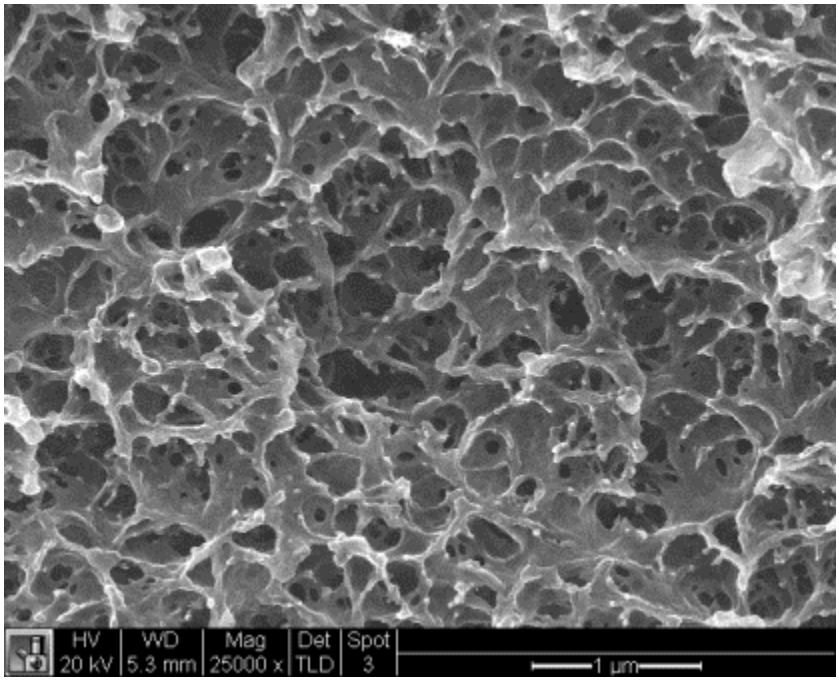

Figure 6.5: SEM image of sample 4.10.1. This sample was foamed for 30 seconds and has an average cell size of 52.8 nm and a relative density of 36.4%.

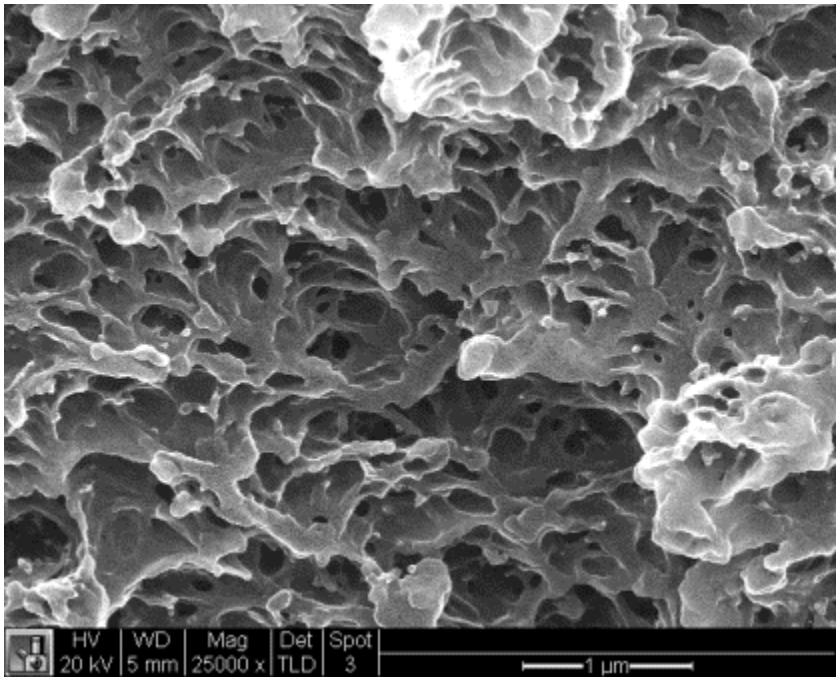

Figure 6.6: SEM image of sample 4.10.9. This sample was foamed for 4.5 minutes and has an average cell size of 99.4 nm and a relative density of 54.0%.

6.4 Discussion

Curvature in foamed samples is expected from oil bath foaming. This is likely due to residual stresses in the material and uneven heating and cooling during foaming. A major reason for using a hot press foaming method instead of an oil bath is to eliminate this curvature. However, samples foamed for short amounts of time in the hot press showed some remaining curvature. Under the conditions studied here, it was found that a sample must be foamed for at least 3 minutes to emerge from the press without residual curvature.

Similar to what is observed in microcellular foaming, the cell size increases with longer foaming times. This means that in using a longer foaming time to ensure flat samples, some sacrifice is made in the final cell size. The smallest average cell size in a flat sample obtained in this experiment was 62.9 nm with a relative density of 48.2%.

The relative density also increases with longer foaming times. This is contrary to what is seen in microcellular foaming in an oil bath, where longer foaming produces larger cells and less dense samples. The press foamed samples cannot grow in the same unconstrained environment as an oil bath. The force of the platens resists this growth and even reduces the thickness of the samples over time. This explains the densification seen in the longer foaming time samples.

Chapter 7 Clamping Force Study

7.1 Introduction

This experiment focused on varying the clamping force of the hot press during foaming. The presence of this force is the most significant difference between this process and oil bath foaming. The clamping force holds the sample in place while foaming and ensures even heating and constrains the sample growth to maintain the desired flatness. However, this force likely also contributes to the perpendicular growth of internal blisters and higher relative densities in the final foam due to physical compression of the plasticized sample. In light of this, the other experiments in this study were conducted with clamping forces at the bottom end of the capabilities of the hot press. The objective of this experiment is to explore this capability range to understand the effects of clamping force on foaming.

7.2 Experiment

All other press foaming experiments used a clamping force of 0.5 tons. For this experiment, the selected clamping forces were 0.1, 0.5, 1, 5, and 10 tons. One sample was foamed at each of the selected clamping forces. The samples were desorbed for between 88 and 107 minutes before foaming. All samples were foamed at 195°C for 3 minutes.

7.3 Results

All samples were successfully foamed in this experiment. The samples foamed at 0.1, 0.5, and 1 ton foamed evenly and maintained their general shape. The samples foamed at 5 and 10 tons deformed significantly during foaming and had different foam structure at the edges than in

the middle, as seen in Figure 7.1. Sample 4.26.2.1, foamed at 0.1 ton had some small blisters at one edge after foaming. Table 7.1 contains the foaming conditions and results of this experiment. Reported values for the 5 and 10 ton samples were measured in the darker central region of the sample.

Table 7.1: Clamping force experiment results.

Sample	Temp C	Clamp Force, tons	Foam Time, m	Desorption Time, m	Mean Thickness, mm	Relative Density	Average Cell Size, nm
4.26.2.1	195	0.1	3	88	1.70	35.5	42
4.26.2.2	195	0.5	3	93	1.53	46.3	43
4.26.2.3	195	1	3	98	1.37	53.9	45
4.26.2.4	195	5	3	103	1.28	45.0	4557
4.26.2.5	195	10	3	107	0.88	56.1	4220

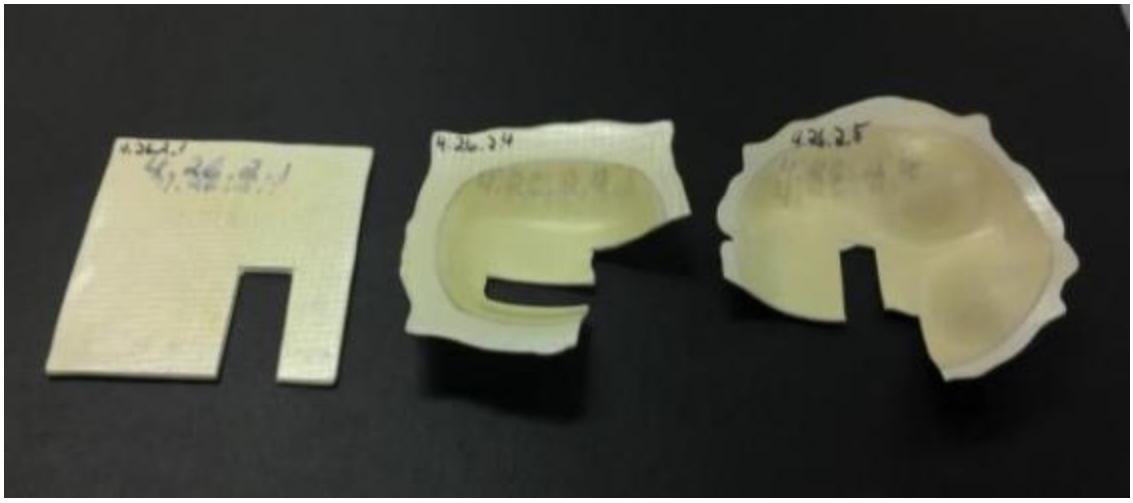

Figure 7.1: Samples foamed at clamping forces of 0.1 tons, 5 tons, and 10 tons, from left to right.

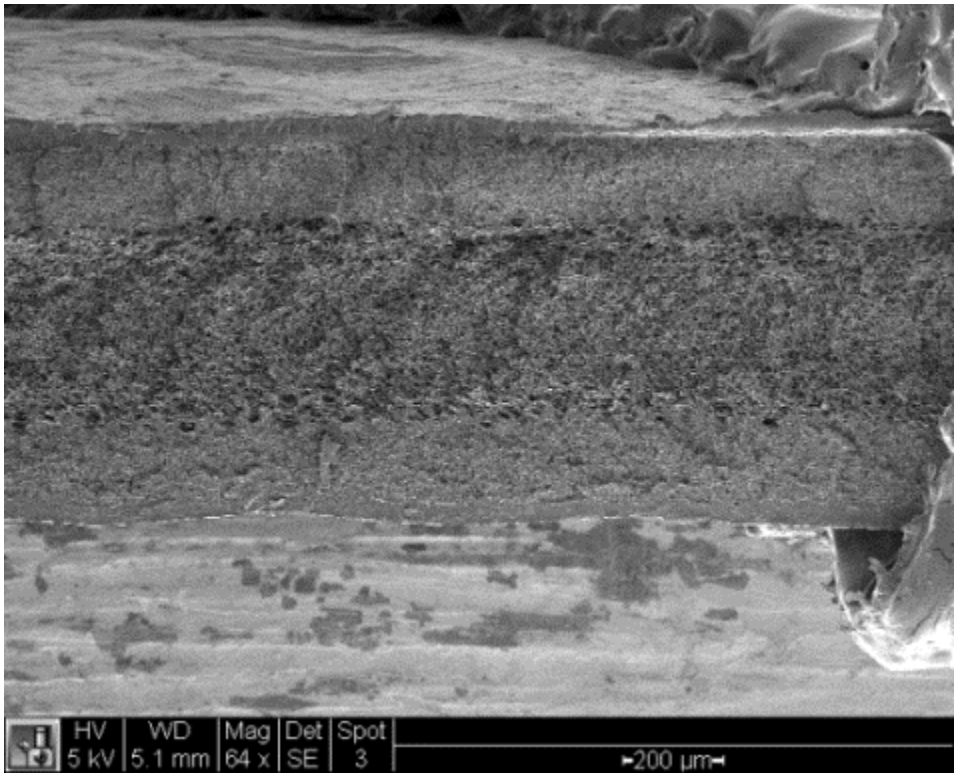

Figure 7.2: Cross-section of sample 2.26.2.5, foamed with a clamping force of 10 tons.

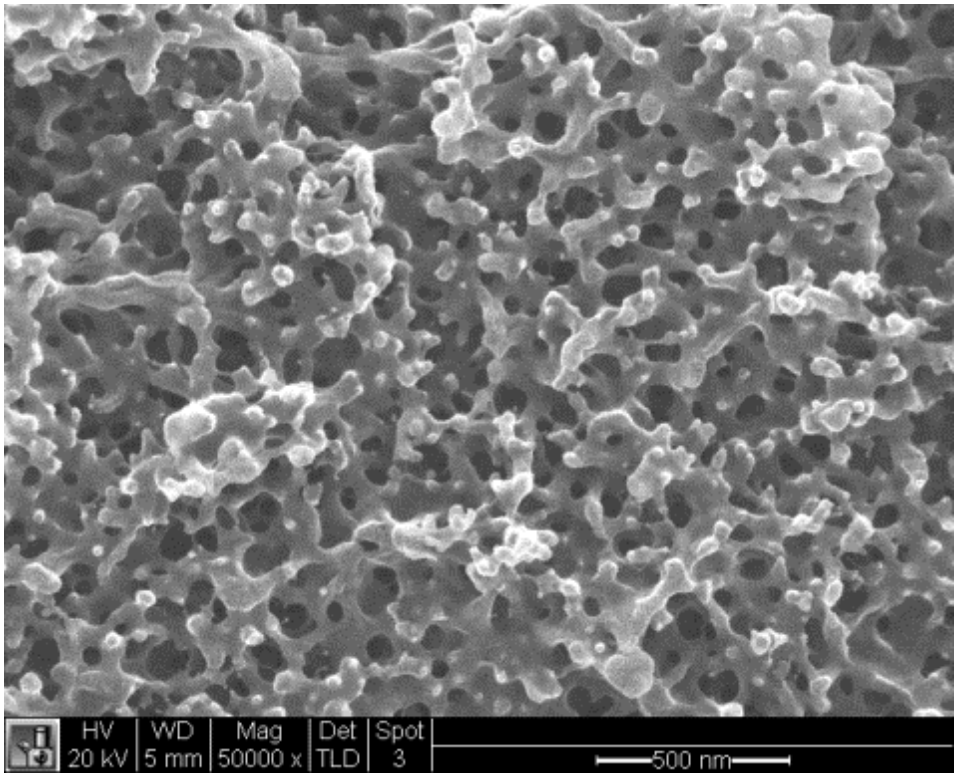

Figure 7.3: Sample 4.26.2.1 nanostructure.

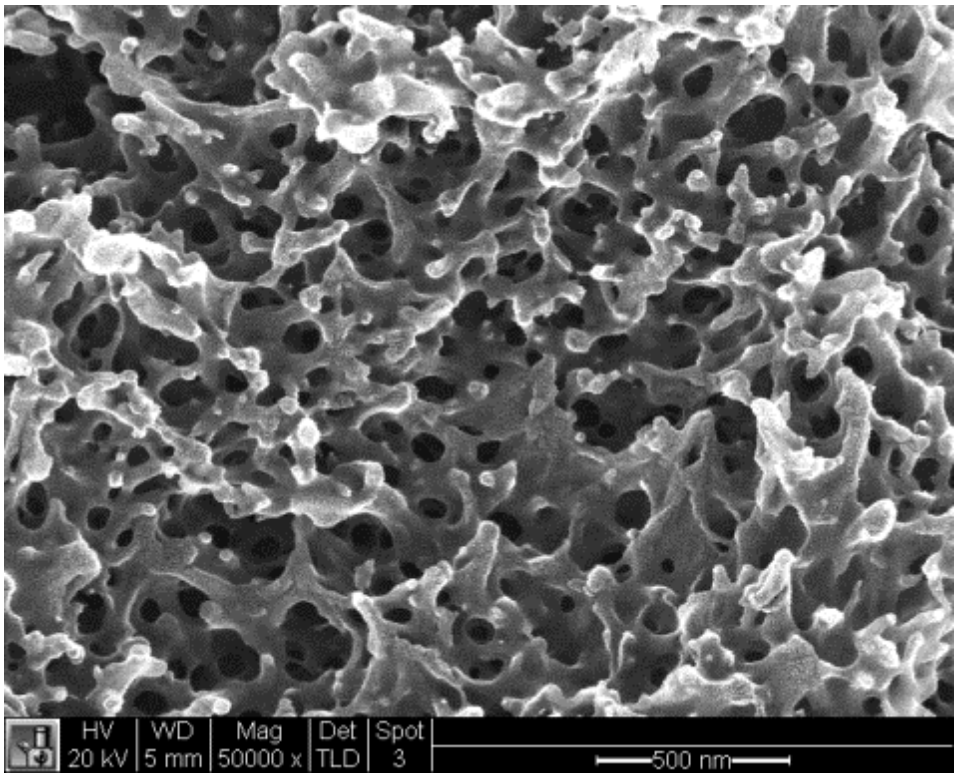

Figure 7.4: Sample 4.26.2.2 nanostructure.

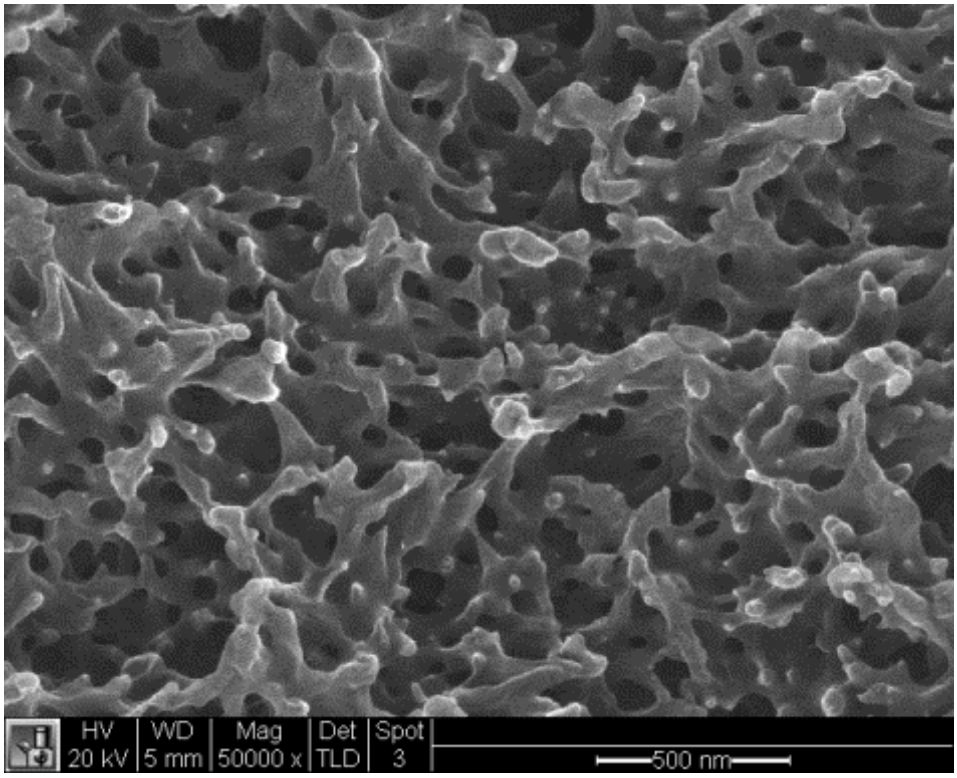

Figure 7.5: Sample 4.26.2.3 nanostructure.

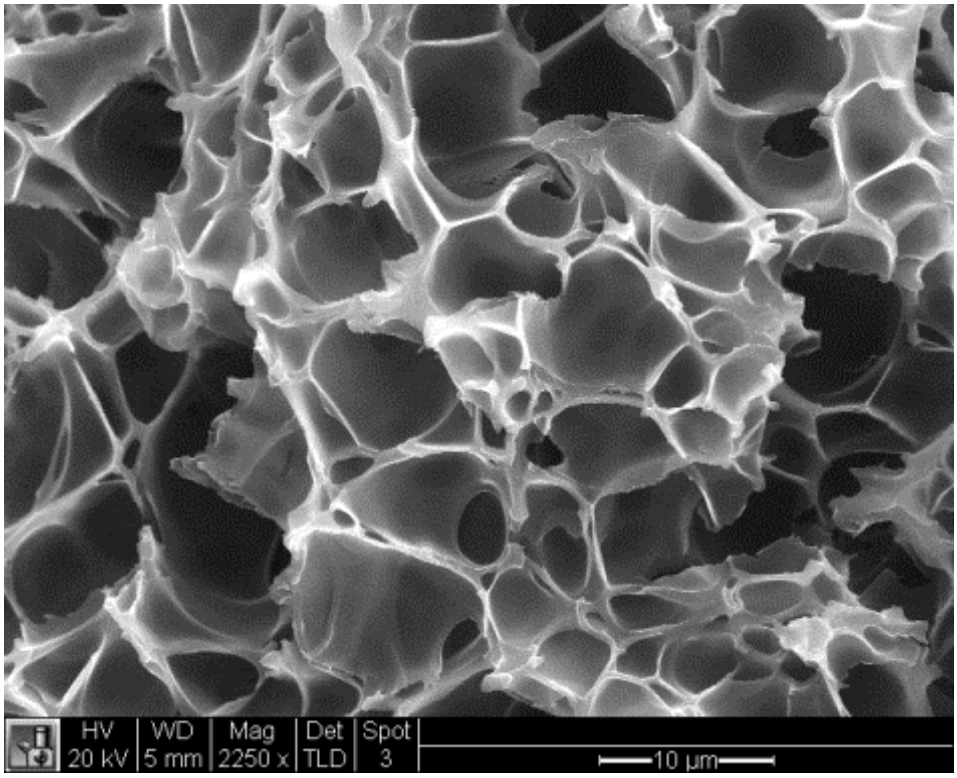

Figure 7.6: Sample 4.26.2.4 microstructure.

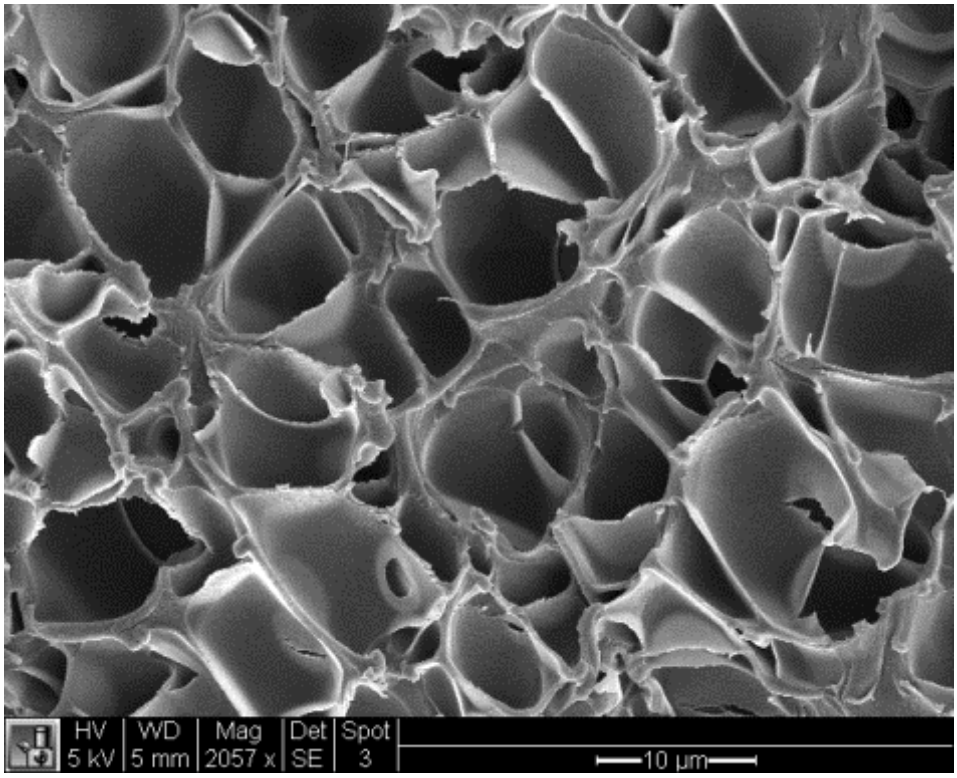

Figure 7.7: Sample 4.26.2.5 core microstructure.

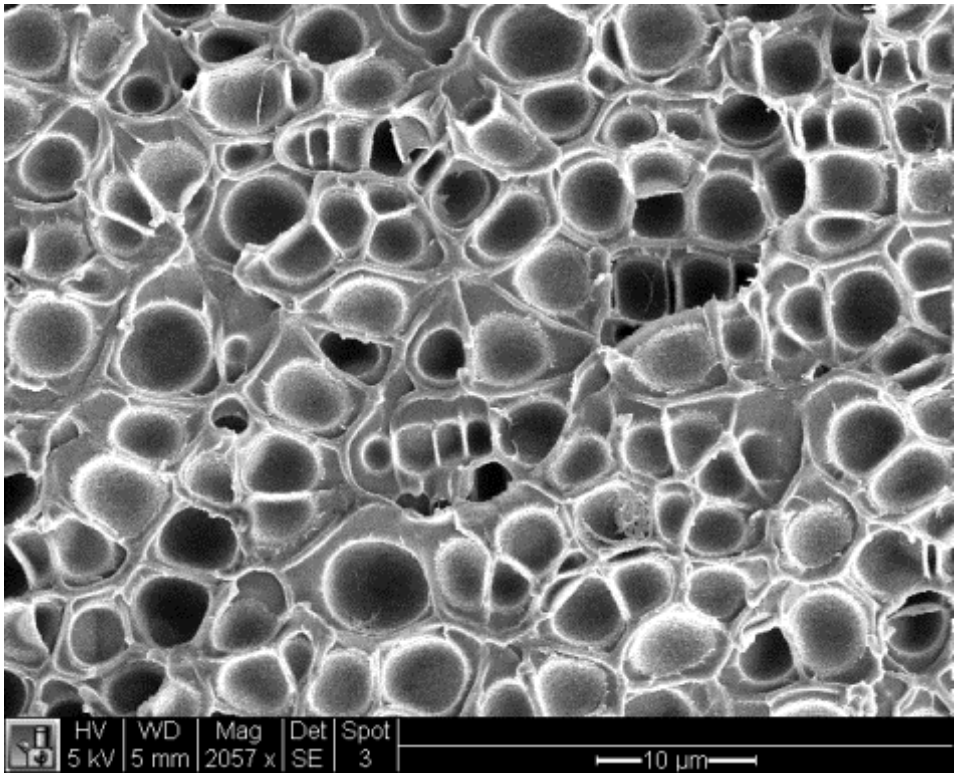

Figure 7.8: Sample 4.26.2.5 transition layer microstructure.

7.4 Discussion

The clamping force clearly has a very significant effect on the resulting foam structure. Between 1 and 5 tons, there is a drastic change in the foam structure with cells growing by two orders of magnitude. The nanocellular sample cell size remained fairly constant, while the relative density grew from 35.5% at 0.1 ton to 53.0% at 1.0 ton and the samples became thinner. The microcellular samples had a transition layer of smaller, denser cells and a core of larger, less dense cells, as seen in Figure 7.2.

The transition to microcellular structures at higher clamping forces reflects the high pressure induced in the foam reducing the number of nucleated cells during foaming. The cells that do nucleate then have more dissolved CO_2 to absorb per cell, causing a greater degree of expansion than in the nanocellular samples. This causes the extreme expansion and curvature seen in the

final samples. This is considered an undesirable result for the purposes of this investigation, but may hold promise in other applications.

There is a clear trend of increasing relative density with increasing clamping pressure until the transition to microcellular foams. This is due to the compressive effect of the press and corresponds to the thickness loss. For the purposes of achieving the lowest relative density and cell size in a flat sample, this experiment suggests that the clamping force should be minimized.

Chapter 8 Foaming Temperature Study

8.1 Introduction

This experiment involved varying the temperature of the hot press platens during foaming. The foaming temperature strongly affects the nucleation of cells in a polymer. The foaming temperature must be above the effective glass transition temperature of the gas-saturated sample in order for foaming to take place. Increasing the foaming temperature beyond this point in oil bath foaming has been shown to reduce the relative density of PEI foams until reaching a minimum around 200°C [3]. A better understanding of the effect of the foaming temperature on nanostructure and relative density will allow for the optimization of the samples that can be created with this process.

8.2 Experiment

Three samples were foamed at each of the 6 selected temperatures for a total of 18 samples. The selected temperatures were 165°C, 175°C, 185°C, 195°C, 205°C, and 210°C. The temperatures were intentionally kept below the original glass transition temperature of the raw PEI. A clamp force of 0.5 tons and a foaming time of 3 minutes were used in this experiment. All samples were desorbed for between 60 and 90 minutes prior to foaming.

8.3 Results

Table 8.1 contains the results of the foaming temperature experiment. Figure 8.1 shows the range of relative densities achieved with various foaming temperatures. The relative density decreases with increasing foaming temperature until reaching a lower limit at 195°C. Sample

3.12.2.5 had the lowest relative density of 42.3%. The relative density rises dramatically between 205°C and 210°C.

The samples foamed at 210°C were significantly reduced in thickness from their pre-foamed state and had significant curvature. They also contain translucent regions that appear to not contain cells, as seen in Figure 8.2. The reported relative density was measured in the opaque parts of the sample.

Table 8.1: Foaming temperature experiment results.

Sample	Temp C	Desorption Time, m	Blistered?	Curved?	Mean Thickness, mm	Relative Density	Average Cell Size, nm
3.12.1.1	165	66	N	N	1.37	65.5%	50
3.12.1.2	165	69.5	N	N	1.40	66.5%	46
3.12.1.3	165	73	N	N	1.30	68.0%	37
3.12.1.4	175	82.5	N	Y	1.48	57.0%	88
3.12.1.5	175	86	N	Y	1.47	58.8%	137
3.12.1.6	175	89.5	N	Y	1.46	59.9%	92
3.12.2.1	185	60	N	Y	1.59	46.9%	50
3.12.2.2	185	63	N	Y	1.59	45.9%	55
3.12.2.3	185	67	N	Y	1.48	47.2%	53
3.12.2.4	195	78	N	N	1.54	43.1%	50
3.12.2.5	195	82	N	Y	1.51	42.3%	59
3.12.2.6	195	86	N	Y	1.58	46.4%	44
3.12.3.1	205	60	Y	Y	1.44	42.8%	36
3.12.3.2	205	63.5	N	Y	1.37	47.2%	48
3.12.3.3	205	67	Y	Y	1.39	45.6%	54
3.12.3.4	210	76	N	Y	0.70	76.1%	57
3.12.3.5	210	80	N	Y	0.76	70.8%	55
3.12.3.6	210	84	N	Y	0.83	73.8%	52

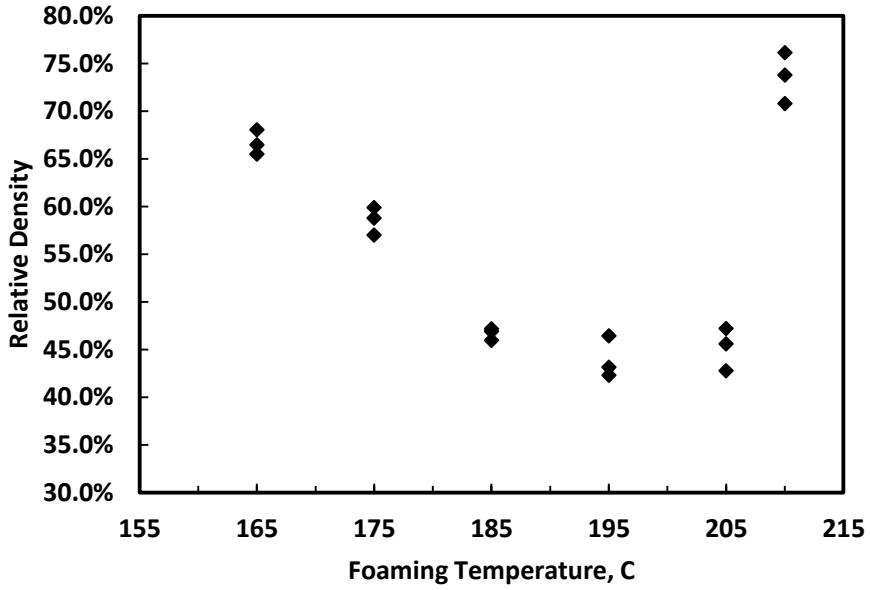

Figure 8.1: Foaming temperature experiment results. Relative density as a function of foaming temperature.

Figure 8.2: Sample foamed at 210°C. The dark circle in the middle is a translucent unfoamed section.

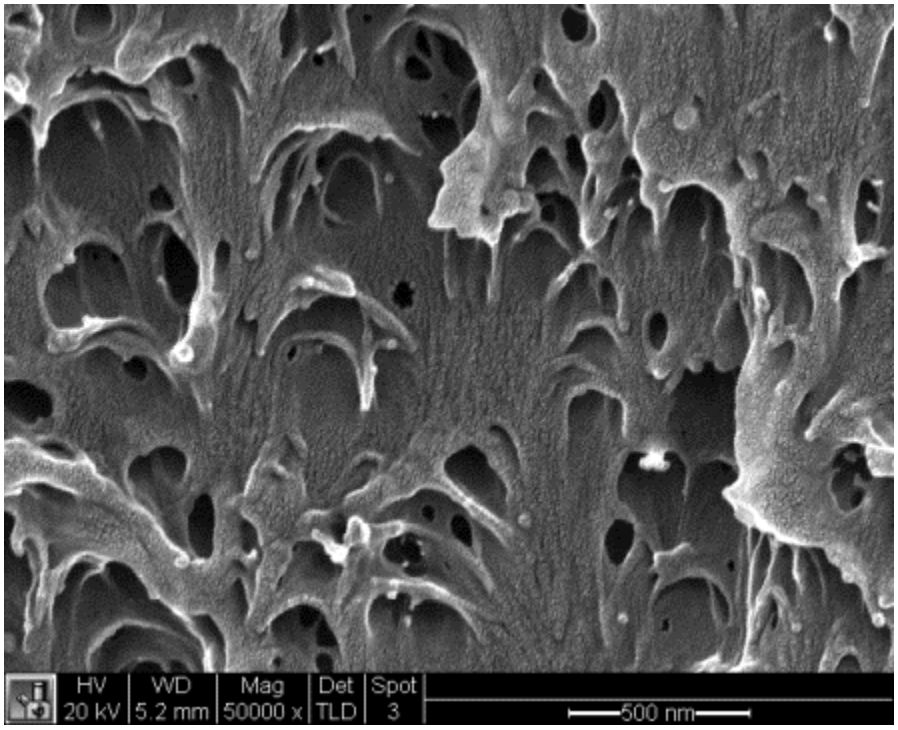

Figure 8.3: Sample 3.12.1.1 nanostructure. This sample was foamed at 165°C.

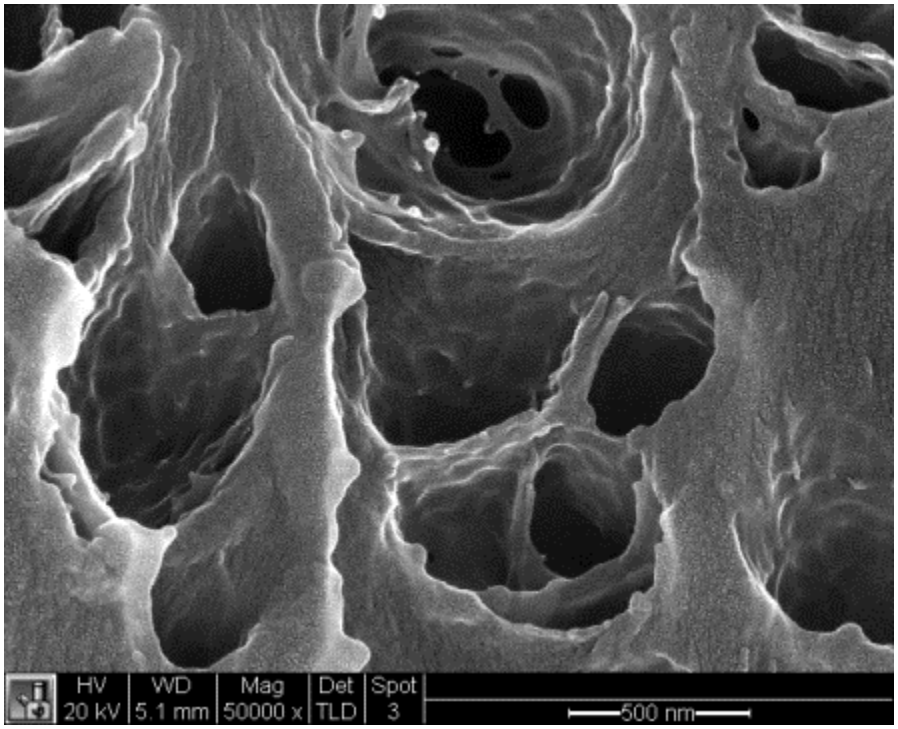

Figure 8.4: Sample 3.12.1.5 nanostructure. This sample was foamed at 175°C.

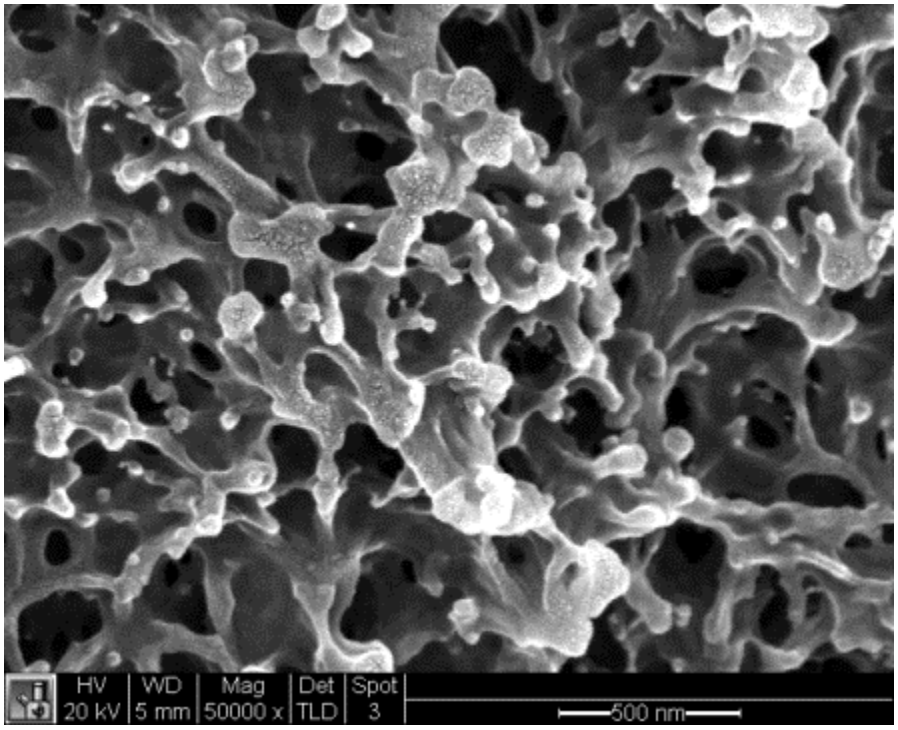

Figure 8.5: Sample 3.12.2.2 nanostructure. This sample was foamed at 185°C.

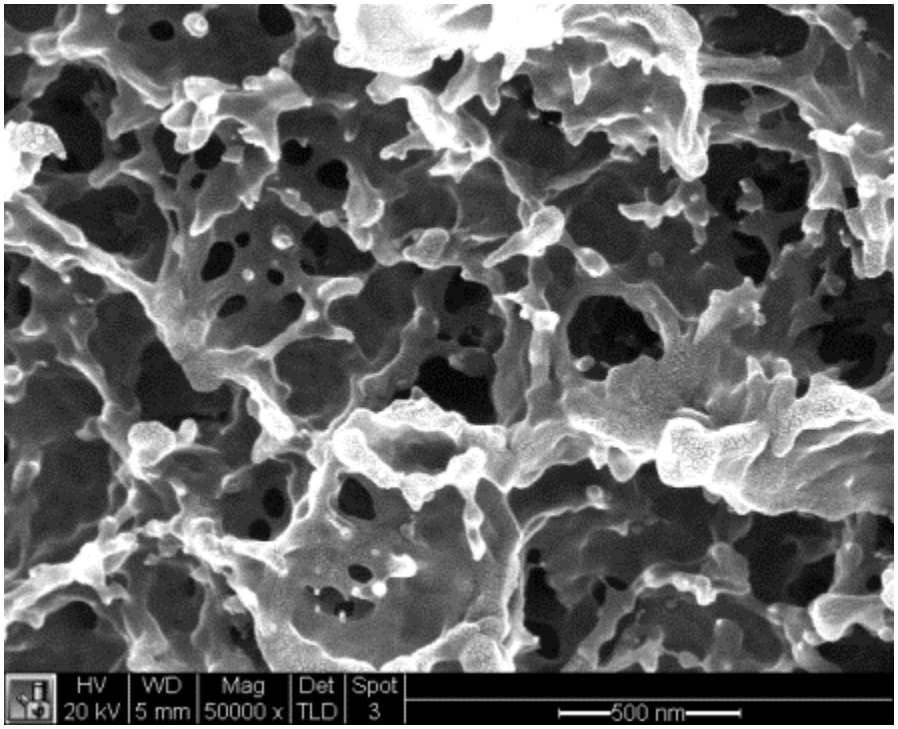

Figure 8.6: Sample 3.12.2.4 nanostructure. This sample was foamed at 195°C.

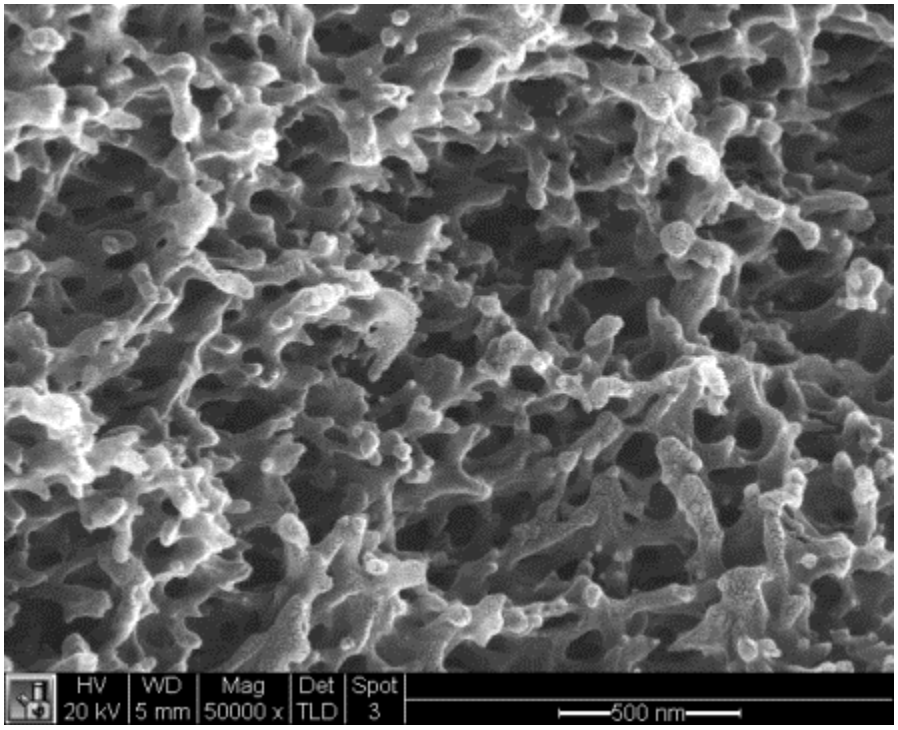

Figure 8.7: Sample 3.12.3.3 nanostructure. This sample was foamed at 205°C.

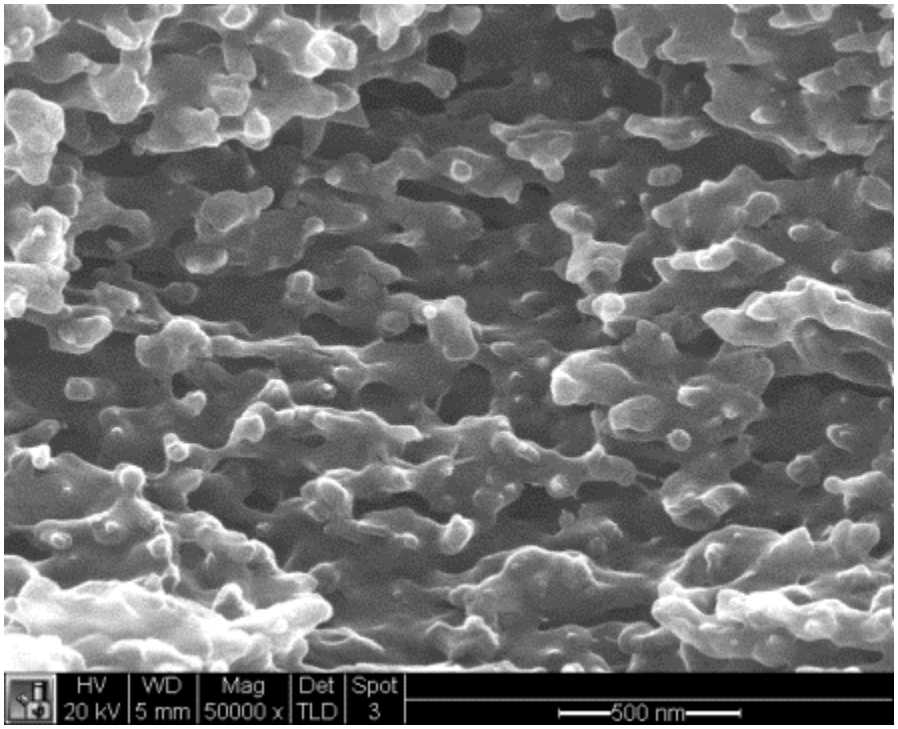

Figure 8.8: Sample 3.12.3.5 nanostructure. This sample was foamed at 210°C.

8.4 Discussion

The relative density of the foamed samples decreases with increasing foaming temperature until the temperature approaches the original glass transition temperature of the polymer. At 210°C, the foam was no longer able to withstand the force of the platens and the foam structure is noticeably compressed, as seen in Figure 8.8. These samples also contained unfoamed areas. The lack of foaming is likely due to locally high pressure from the clamping force preventing nucleation. This represents the upper limit of foaming temperature in this process. Temperatures between 195°C and 205°C, however, produce nanocellular foams of low density.

This range of foaming temperatures shows a variety of nanostructure morphologies. The samples foamed at 165°C and 175°C show relatively large voids with nanoscale openings between them. Samples foamed at 185°C and 195°C show smaller voids with similarly sized nanoscale openings. The samples foamed at 205°C show relatively homogeneous interconnected nanoscale cells. Finally, the samples foamed at 210°C show a compressed nanostructure with far fewer cells. The average cell sizes of these samples, as measured by the procedure outlined in section 2.5.4 , are fairly constant around 50-100 nm.

Chapter 9 Preliminary Experiments in Solid Skin Removal

9.1 Introduction

This chapter discusses preliminary experiments in removing the solid skin and transition layers from nano-foamed samples. The methods investigated herein involved physically abrading the surface of the samples to reduce the sample thickness and expose the nanocellular core. The challenge was to physically remove the solid and microcellular regions without significantly damaging the porous core region. The samples produced by these methods were tested qualitatively for their ability to absorb liquids.

9.2 Experimental Methods

The methods of skin removal chosen in this experiment included machining and polishing. Machining experiments were conducted on a standard 3-axis turret mill. A sharp steel, 4-flute end mill was used for machining the sample surface. The samples were adhered to a metal block using 3M brand double-sided carpet tape. The metal block was leveled and clamped into the milling table to hold the sample for machining. Milling speeds ranged from 1400-1800 rpms. The samples surfaces were machined in successive passes of distinct cutting depths, ranging from 0.10-0.30 mm. The feed rate of each pass was controlled by hand and could not be measured.

Figure 9.1: Buehler EcoMet 250 Grinder-Polisher used in polishing experiments.

The polishing experiments were conducted on a Buehler EcoMet 250 Grinder-Polisher similar to that shown in Figure 9.1. These machines are primarily designed for polishing metal surfaces to mirror finishes. The machine holds a sample against a polishing wheel with a set force while spinning the sample and the wheel at set speeds. A water jet wets the surface of the polishing wheel during the process. For these experiments, a diamond polishing pad was used to abrade the samples. The samples must be adhered to the surface of a hard steel cylinder using the carpet tape to be held by the sample arm of the machine. These experiments were conducted with a sample force of 1 pound, a polishing wheel rotation of 80 rpm, and a sample rotation of 40 rpm.

Both methods require the use of double-sided tape to hold the sample during skin removal. The samples were separated from the tape by dissolving the tape glue in acetone. The nanoporous core must be exposed on both sides in order to be used as a battery separator. This requires two polishing or machining steps, each of which requires the sample to be held strongly

in place. Since the desired resulting membrane will be extremely thin, it is necessary to remove the sample from its holder without damaging it.

In order to investigate the extent of open porosity in the abraded samples, experiments were undertaken to visualize the sample's absorption of liquid through the abraded surface. The abraded surfaces all showed considerable hydrophobicity, so water could not be used as the absorbed liquid. Instead, acetone was mixed with permanent black dye from a Sharpie marker and applied to the abraded surfaces using an eye dropper. The absorption of this liquid into the surfaces was observed qualitatively. PEI is rated as having some observed effect after 7 days of exposure to acetone at room temperature. To distinguish the absorption of this solvent into the nanoporous core from a chemical interaction between the two, control experiments were undertaken to observe the interaction between acetone and solid PEI. Acetone droplets were applied to the surface of an unprocessed PEI sample and the unpolished surface of a nanocellular sample. In both cases, no absorption into the polymer was observed before the acetone evaporated.

9.3 Results

The machining experiments were successful in removing the solid skin from the foamed samples. Figure 9.2 shows one of the machined samples. The machined surfaces are very rough, with numerous gouges, especially near the edges. The forces involved in machining caused the sample to vibrate and lead to warped, jagged machined samples. SEM images of the machined surface show jagged cuts from the mill, with the underlying cellular structure highly disturbed and solidified. Porosity testing showed limited absorption of acetone and dye into these surfaces.

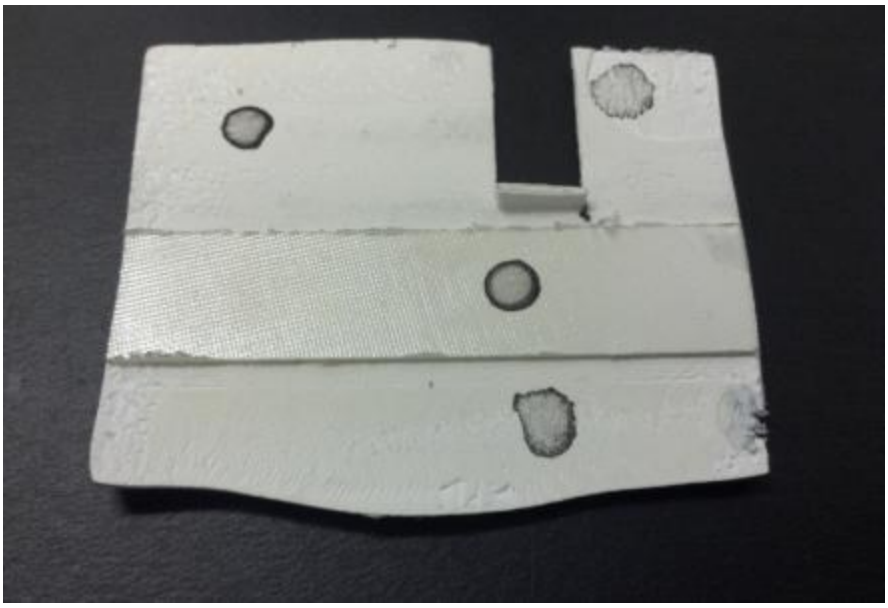

Figure 9.2: Machined surface of a sample. The textured horizontal stripe has not been machined. The vertical rectangle was removed for SEM imaging. The black dots are ink stains from porosity testing.

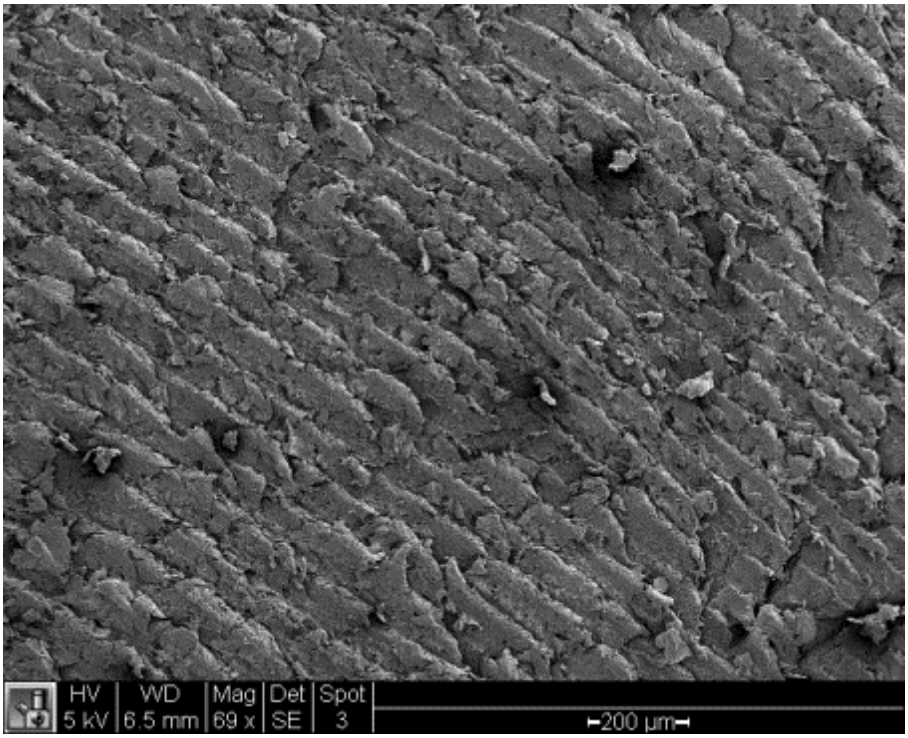

Figure 9.3: SEM image of sample surface machined at 1400 rpms and a thickness removal of 0.15 mm.

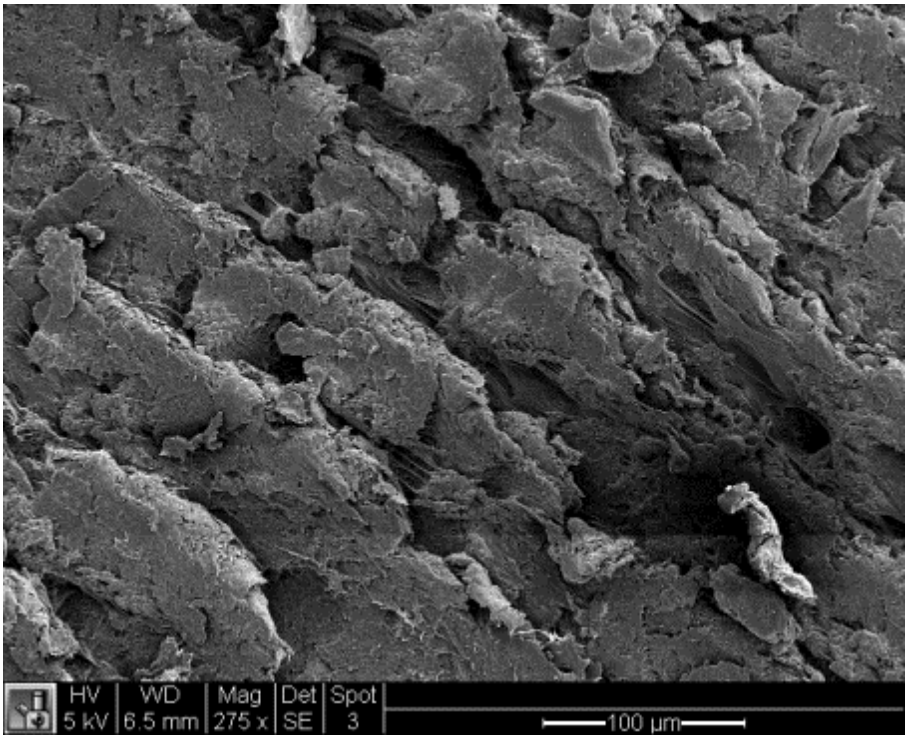

Figure 9.4: SEM image of sample surface machined at 1400 rpms and a thickness removal of 0.15 mm.

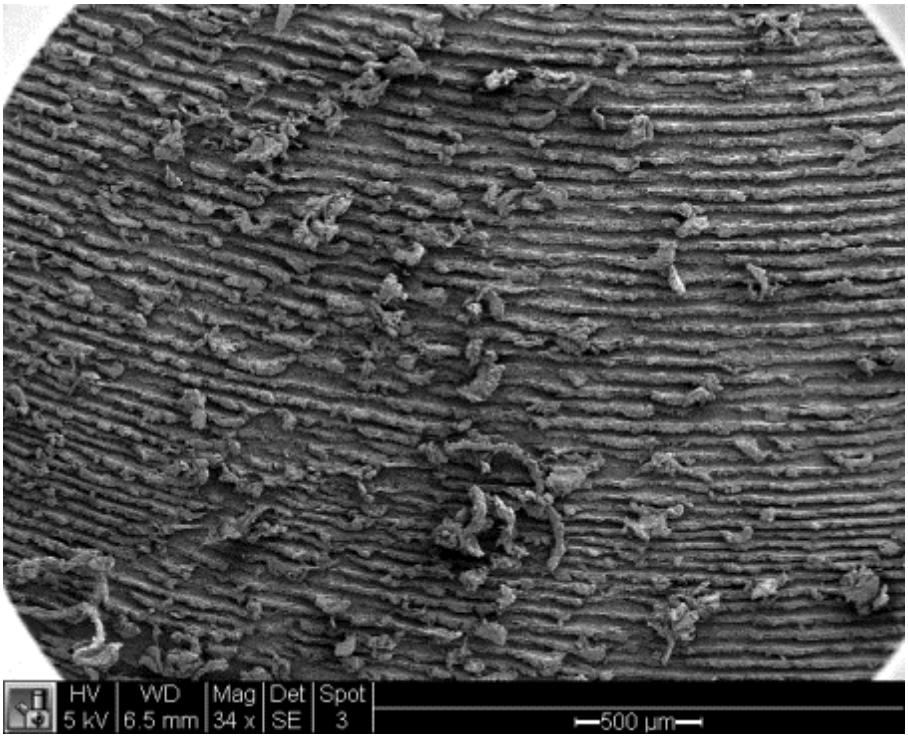

Figure 9.5: SEM image of a sample surface machined at 1800 rpms and a total thickness removal of 0.40 mm in 0.10 mm increments.

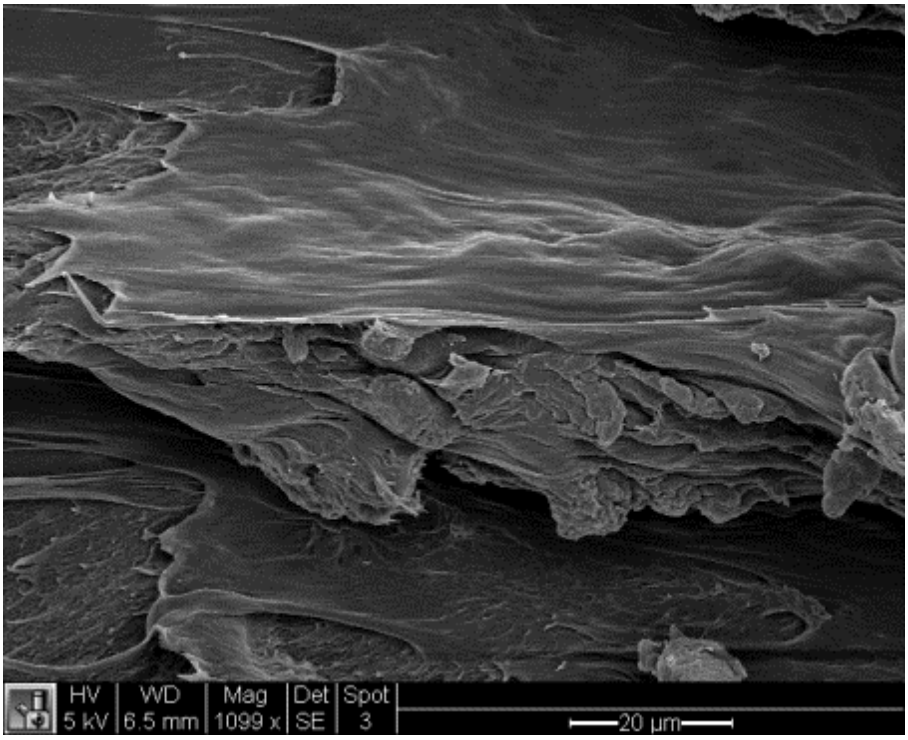

Figure 9.6: SEM image of a sample surface machined at 1800 rpms and a total thickness removal of 0.40 mm in 0.10 mm increments. This image shows evidence of a distorted porous structure that has been partially solidified by the milling process.

The polishing experiments resulted in thin, relatively smooth samples with controllable thicknesses. Figure 9.7 shows two samples with polished surfaces. Both samples had an original thickness of 1.61 mm. Sample 1 was polished for 1.5 minutes on each side and had a final thickness of 1.10 mm. Sample 2 was polished for 3.5 minutes on each side and had a final thickness of 0.65 mm. This suggests an average thickness removal speed of 0.15 mm per minute of polishing. The thicker sample did not show evidence of porosity in absorption tests. The thinner sample absorbed acetone and dye readily.

SEM images of the polished surface show regions of smooth solid polymer interspersed with regions of exposed porosity, often aligned with the direction of rotation during polishing. Cross-sectional SEM images show a thin solid layer at the polishing surface. Figure 9.10 shows that Sample 1 was polished down to the transition layer. The transition layer cells close to the surface

have been dramatically collapsed by the pressure of the polishing process, forming the solid layer seen in the surface images. Figure 9.14 shows that Sample 2 has been polished down to the nanocellular core. A similar solid layer can be seen at the polished surface of Sample 2. However, the nanocellular core does not appear to be collapsed beyond the solid layer.

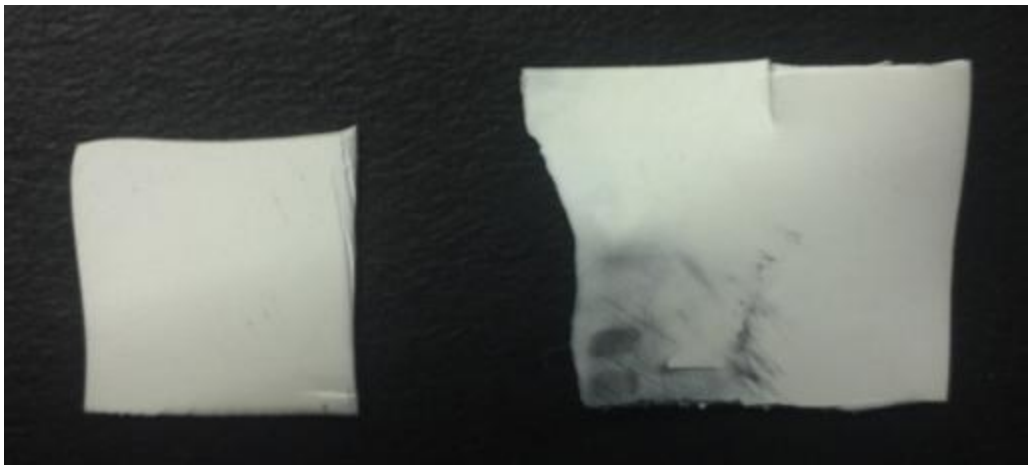

Figure 9.7: Samples with polished surfaces. The samples have final thicknesses of 1.10 mm on the left (Sample 1) and 0.65 mm on the right (Sample 2). The visible ink stains on Sample 2 are from porosity testing.

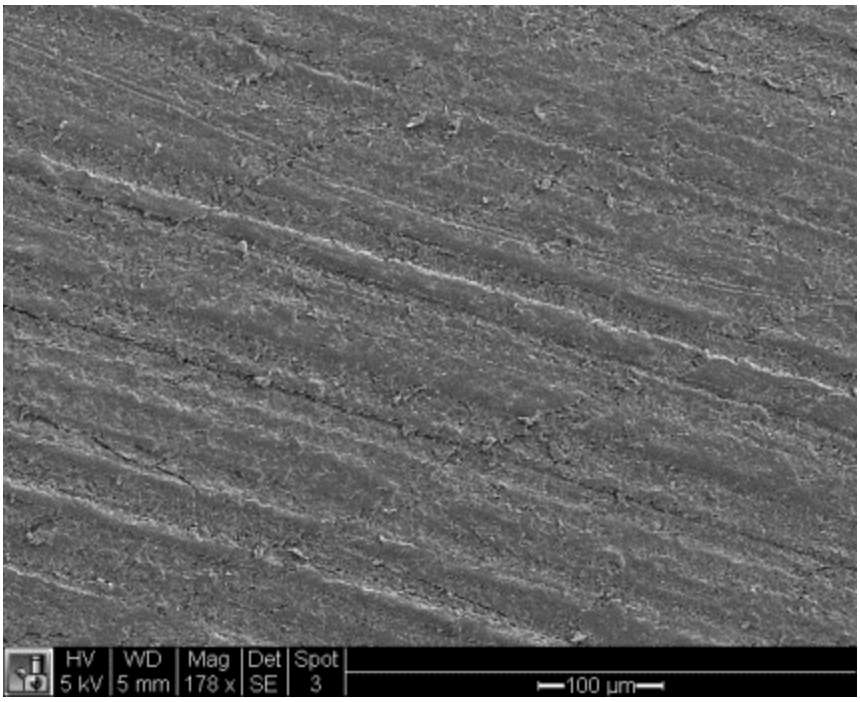

Figure 9.8: SEM image of the polished surface of Sample 1.

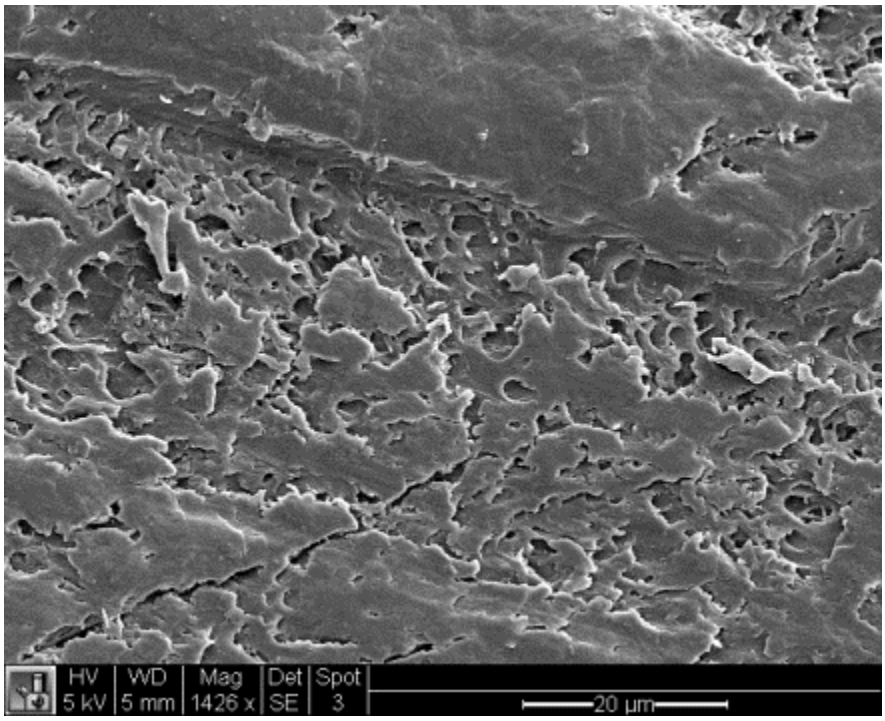

Figure 9.9: SEM image of the surface of Sample 1. Note the solid region at the top of the image and the more porous region in the middle.

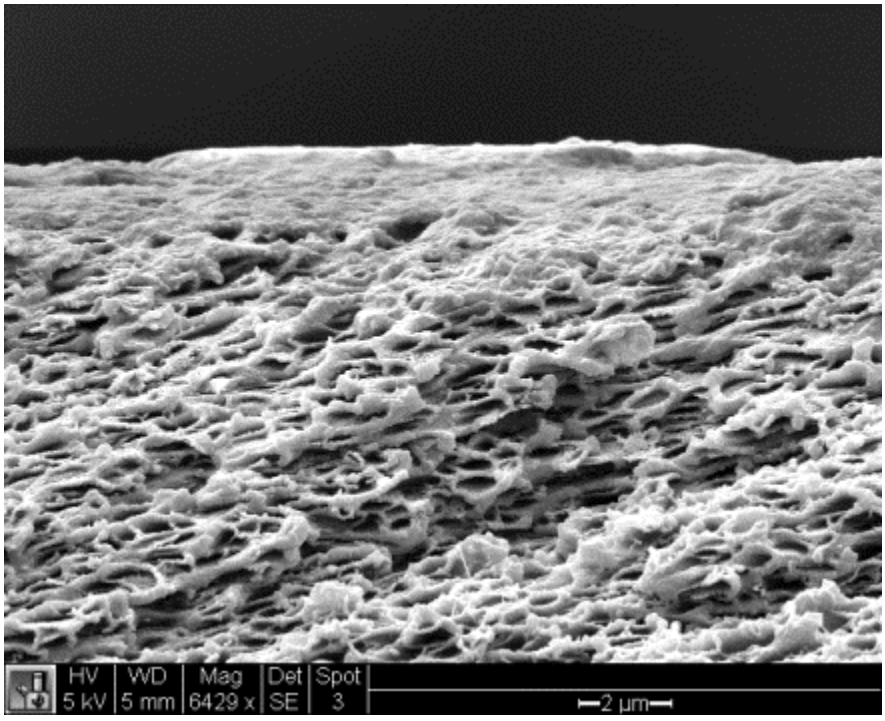

Figure 9.10: SEM cross-sectional image of the polished surface of Sample 1. The thin polished surface can be seen at the top of the sample, with microcellular transition layer cells beneath.

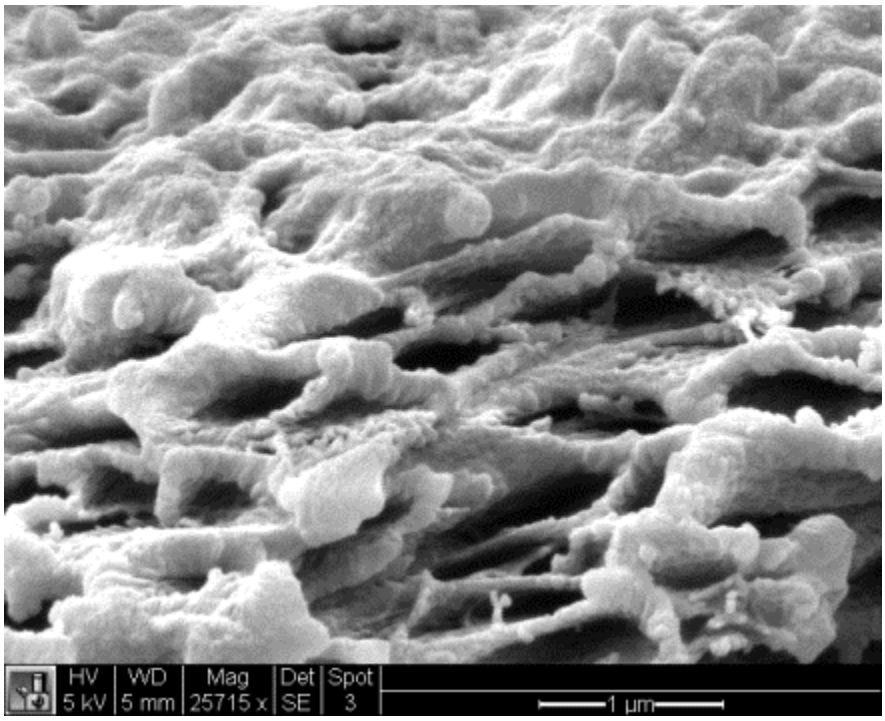

Figure 9.11: SEM cross-sectional image of Sample 1, showing the considerable collapse of transition layer cells in the polishing process.

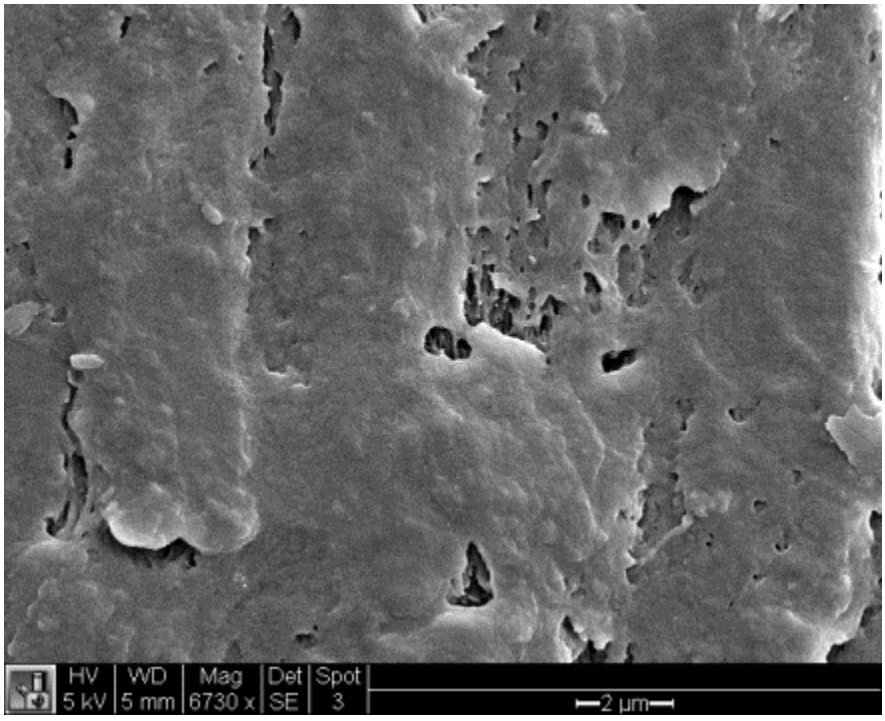

Figure 9.12: SEM image of the surface of Sample 2. This image is of a relatively less porous region.

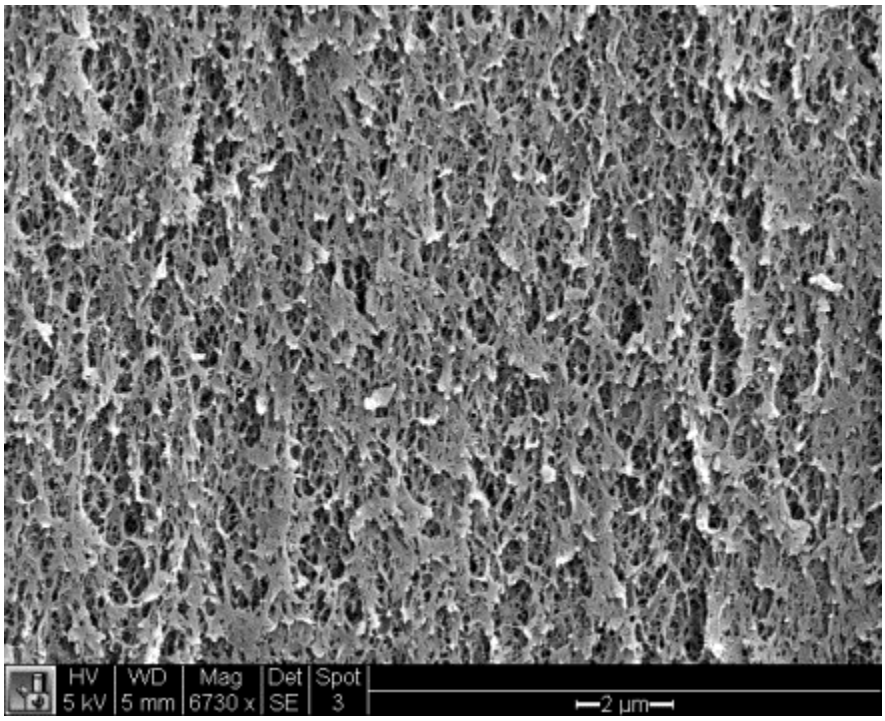

Figure 9.13: SEM image of the surface of Sample 2. This image shows a very porous region of the polished surface.

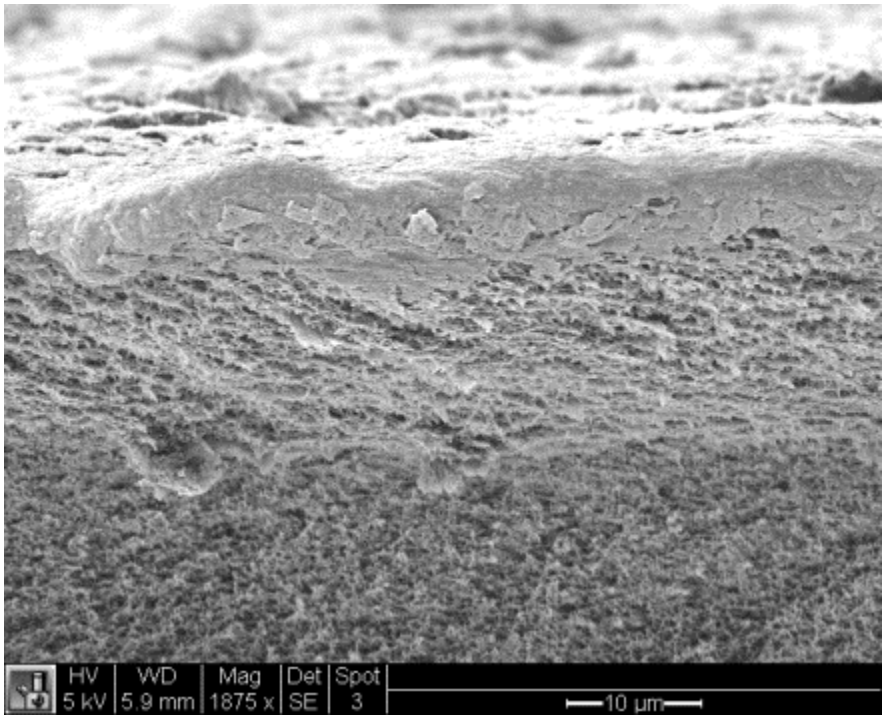

Figure 9.14: SEM cross-sectional image of Sample 2. The polished surface appears at the top of the image, over nanoporous core cells.

9.4 Discussion

The machining process does not appear to be a viable method of removing the solid skin from samples foamed in this process. The mill produced jagged, rough surfaces with uneven thicknesses. Furthermore, these surfaces did not appear to have exposed the porous core of the samples. An advantage of the machining process is that mills have a large area of operation and could easily be applied to larger samples.

Polishing does appear to be a promising method of producing porous surfaces on these samples. The polishing process produces flat, smooth samples with relatively constant thickness. The thickness removed from the sample can be easily controlled to produce samples of desired thicknesses. A drawback of the polishing machine used in this experiment was the small sample size necessary.

Both methods succeeded in physically removing the solid skin layer from the sample. However, both methods reproduce a solid skin on the new surface of the sample. This skin is composed of cellular regions that have been compressed back into a solid by the force of the abrasion. Encouragingly, this skin is not uniform, leaving holes and porous regions that expose the underlying porous structure. It is possible that certain polishing pads and conditions could reduce or eliminate this induced solidification, leaving a perfectly porous surface.

These experiments confirmed the suspicion that the nanocellular foam structure has an open porosity. The samples readily absorb acetone as compared to solid PEI. Experiments with dyed acetone showed dye penetrating one polished surface and emerging from the opposite surface shortly thereafter. However, it is important to note that these samples are hydrophobic, and so could not be used in an aqueous battery without further modification. Interestingly, these

samples also absorb liquid nitrogen. This phenomenon was noticed while preparing the samples for SEM imaging. It is unknown whether the absorbed liquid nitrogen has any effect upon the fracture surface.

The thinnest sample produced in preliminary polishing experiments was 80 μm thick. There remains a significant challenge in reducing this final thickness to the desired 25 μm. Further experiments are necessary to discover processing and handling methods that yield films of the desired thickness with uniformly porous surfaces. In addition, procedures for the handling and characterization of the thin films without damaging the structure must be developed.

Chapter 11 Conclusions and Recommendations

11.1 Conclusions

This thesis contains an investigation into the preparation of flat, non-blistered, nanocellular samples. The process developed herein involves the use of supercritical CO_2 to accelerate the saturation process and a hot press foaming method to produce flat samples. The critical parameters of this process are the saturation pressure, saturation temperature, desorption time, foaming time, clamping force, and foaming temperature.

Preliminary experiments in foaming thin films directly did not succeed in eliminating the solid skin layer. The novel in situ foaming apparatus does not have a sufficient heating rate to eliminate desorption prior to foaming from the process. Furthermore, the foams produced in these experiments did not have open nanoporous features.

The saturation temperature and pressure strongly affect the resulting foam structure. Previous work in the Microcellular Plastics Laboratory has characterized the gaseous CO_2-PEI system at pressures between 1 and 5 MPa at room temperature [3]. The use of pressures and temperatures in the supercritical range of CO_2 in this investigation was motivated by an expected reduction in the necessary saturation time. The conditions used for all samples in this thesis were 20 MPa and 45°C, which result in similar equilibrium CO_2 concentration as 5MPa and 23°C but with reduced saturation time.

The desorption time controls the final CO_2 concentration distribution across the sample at the time of foaming. The concentration distribution strongly influences the core cell structure, skin layer thickness, and transition layer thickness. This investigation found that the desorption time is critical to reducing the formation internal blisters through a mechanism that is not fully

understood. The desorption study results found that if the samples are allowed to desorb for at least 35 minutes, the rate of internal blistering is very low. Critically, this amount of desorption leaves a nanocellular core in place.

The foaming time controls the nucleation and growth of the cells within the sample. The foaming time experiment suggests that longer times in the press lead to larger average cell sizes. However, the longer exposure to the external compressive force of the press causes the samples to become denser. Thus, in seeking to produce a sample with minimal average cell size and density, the foaming time should be as small as possible. However, shorter foaming times were found to strongly affect the flatness of the foamed sample. This is likely due to the relaxation of internal stresses caused by cell nucleation and growth. The foaming time must be carefully selected to produce flat samples with the desired cellular structure.

The clamping force holds the sample in place during foaming and constrains its growth to a plane. However, higher clamping forces result in thinner, denser samples. For the production of samples using this process, the lowest clamping force possible should be used. However, further study into the use of clamping force in foaming could provide interesting results. Specifically, higher clamping forces combined with high temperatures and foaming times may be utilized to produce foamed thin films from thicker sheets. This may be a solution to the inherent issues of using the microcellular process on thin films, where rapid desorption limits the process.

The foaming temperature and gas concentration largely determine the structure of the foam. In press foaming, the temperature is bound by the glass transition temperature of the raw PEI (217°C). As the foaming temperature approaches this transition, the samples lose thickness and become denser, even failing to foam in some locations. This experiment found that the relative density of the samples was lowest at 195°C. Several nanoscale morphologies can be achieved

with small changes in the foaming temperature. Further exploration into the properties of these morphologies would be possible using samples made with this process.

Preliminary attempts to remove the solid skin and transition layers through physical abrasion were successful. Machining the sample surface using standard milling techniques produced jagged, warped surfaces with poor acetone absorption characteristics. Polishing the sample surface showed more promise, producing flat, even surfaces that readily absorbed acetone and dye. Critically, these experiments confirmed that the nanocellular core structure is open and porous.

11.2 Summary of Observations

- Preparing nanocellular PEI samples for SEM imaging requires freeze fracturing samples in liquid nitrogen. During sample preparation for this study, it was noticed that the fracture behavior of these samples was not isotropic. Flat fracture surfaces could only be obtained on one fracture plane, with jagged surfaces resulting from attempts to fracture on other planes.
- During liquid nitrogen fracturing, it was noticed that the nanocellular samples absorbed liquid nitrogen through fracture surfaces. After removal from the nitrogen bath, this absorbed liquid could be seen dripping out of the nanostructure. This represents another confirmation of the open porosity of this structure.
- The traditional means of characterizing microcellular foams involves measuring the average cell size and nucleation density from SEM images. This model fails to accurately represent the structure of open nanocellular foams. In the majority of the samples produced in this research, the nanostructure consists of a complicated network of interconnected voids. No clear cell walls are present to guide cell diameter measurement or cell counting. Thus, there

exists an opportunity for developing a new characterization method to understand and compare nanocellular structures.

11.3 Recommendations

The process developed in the course of this research represents a viable method for reliably and quickly producing flat nanocellular PEI samples. These samples may be used for future study into the properties of nanofoams and the specific application of battery separators. In addition, further research into the limitations of the saturation and foaming process could yield improvements in nanostructure and processing time.

The preliminary experiments in in situ foaming of thin films showed that desorption has not been fully eliminated from this process. The reason for this failure was the slow heating rate of the sample surface during foaming. Desorption occurs as the sample temperature increases prior to reaching the threshold foaming temperature. A possible method of avoiding this problem would involve flooding the pressure vessel with a preheated liquid or gas. This would guarantee instantaneous heating of the sample surface. However, this process would have to take place without reducing the pressure on the sample.

The use of supercritical CO_2 as a saturation medium shows promise in reducing the necessary saturation time and increasing the saturation concentration. Future research could seek to further increase the saturation concentration with higher saturation pressures and lower temperatures. Higher CO_2 concentrations may lead to smaller nano-scale features and lower relative densities. In addition, the effect of temperature on the saturation concentration should be characterized.

The hot press foaming method results contained herein raise a number of unanswered questions that warrant further investigation. First, the significant effect of higher clamping forces

on the nanostructure demands additional experimentation. More resolution is necessary to observe the transition from nanocellular structure to the dual layer microcellular structure seen in higher clamping force samples. Second, the effect of desorption time on the thickness of the transition layer and skin layer presents an opportunity to understand the transition from microcellular transition layer cells to interconnected nanostructure. If the gas concentration at the moment of foaming can be predicted, the threshold conditions for this transition can be quantified and understood. Finally, these experiments involved foaming one sample at a time. Future experiments could focus on attempting to foam multiple samples simultaneously to avoid the effects of different desorption times between samples and make the process more economically viable.

The fundamental physical process that results in an open, interconnected nanostructure is not presently understood. It has been conjectured that this phenomenon is caused by a fundamental difference in the physical mechanism of foaming, from nucleation and growth of cells to a phase separation phenomenon known as spinodal decomposition. Critically, if the parameters that control this shift in foaming method can be controlled, it may be possible to produce closed cell nanocellular foams with better thermal insulation properties.

The thermal and mechanical properties of these samples could be investigated. Theoretical improvements in the thermal insulation properties of nanofoams can be assessed by thermal conductivity testing.

Finally, the potential for these samples to be processed into battery separators should be investigated. The polishing method of solid skin removal should be further refined to produce thin, open porous battery separators. The properties of these processed samples should be studied to assess their suitability for the battery separator application.

List of References

1. Martini, J., Waldman, F. A., and Suh, N. P. "The Production and Analysis of Microcellular Foam." SPE Tech. Papers, XXVIII (1982): 674-676.
2. Kumar, V. "Microcellular Foams." In Handbook of Polymer Foams, by Ed. David Eaves, 243-267. Shropshire, UK: Rapra, 2004.
3. Miller, D and Kumar, V. "Microcellular and nanocellular solid-state polyetherimide (PEI) foams using sub-critical carbon dioxide I. Processing and structure." Polymer, 50 (2009): 5576-5584.
4. Miller, D and Kumar, V. "Microcellular and nanocellular solid-state polyetherimide (PEI) foams using sub-critical carbon dioxide II. Tensile and impact properties." *Polymer*, 52 (2011): 2910-2919.
5. Krause, B. "Bicontinuous Nanoporous Polymers by Carbon Dioxide Foaming." Macromolecules, 34 (2001): 8792-8801.
6. Zhou, C, Vaccaro, N, Sundarram, S S, and Li, W. “Fabrication and characterization of polyetherimide nanofoams using supercritical CO2.” Journal of Cellular Plastics, 48 (2012), 239-255.
7. Zhang, S. “A review on the separators of liquid electrolyte Li-ion batteries.” Journal of Power Sources, 164 (2006): 351-364.
8. Nadella, K, Kumar V, Li, W. “Constrained Solid-State Foaming of Microcellular Panels.” Cellular Polymers, 24 (2005): 71-90.
9. Miller, D. “Characterization of Polyetherimide Carbon Dioxide System and Mechanical Properties of High Relative Density Polyetherimide Nanofoams.” MS Thesis. University of Washington, Seattle (2007).
10. Montecillo, R. “Feasibility of Producing Microcellular Thin Films in the Polycarbonate-Carbon Dioxide System.” MS Thesis. University of Washington, Seattle (1994).
11. Lu, J. “Processing and Characterization of Thermoplastic Microcellular Thin Films.” MS Thesis. University of Washington, Seattle (2008).